THE PENNSYLVANIA STATE UNIVERSITY
SCHREYER HONORS COLLEGE

DEPARTMENT OF INDUSTRIAL AND MANUFACTURING ENGINEERING

DISCRETE ELEMENT METHOD (DEM) MODEL CALIBRATION TECHNIQUES FOR ADDITIVE MANUFACTURING

KRISTEN NICOLE MEIHOFER
SPRING 2018

A thesis
submitted in partial fulfillment
of the requirements
for a baccalaureate degree
in Industrial Engineering
with honors in Industrial Engineering

Reviewed and approved* by the following:

Sanjay Joshi
Professor of Industrial Engineering
Thesis Supervisor

Catherine Harmonosky
Associate Professor of Industrial Engineering
Honors Advisor

* Signatures are on file in the Schreyer Honors College.

ABSTRACT

Powder bed fusion is a commonly used Additive Manufacturing technique. This technique uses a layer-by-layer approach to create the desired part in 3D printing, where the layers are created by spreading a thin layer of powder. The ability to simulate this process would give scientists the opportunity to visualize this process before printing the part, allowing them to best utilize the capabilities of powder bed fusion. Spreading of the powder to create the layer to be fused is the first step in the process, and the quality of the layer can impact the building of the part. The overall goal of this research is to investigate the use of simulation models for the spreading of the powder. However, before this simulation is possible, the required simulation inputs must be understood, and the model calibrated. Calibration of the simulation models is the focus of this research. The simulation inputs are based on the powder used in the process. Powder characterization tests are run to understand properties about the powder. One of the most common, due to its simplicity, is the angle of repose test. This paper develops an efficient calibration model for the simulation of the angle of repose test using the discrete element method. The discrete element method (DEM) is the basis to calculate how the particles react when they collide with other particles or equipment. A commercial DEM software, EDEM, is used to simulate the DEM for this experiment. This calibration technique efficiently calibrates the input variables associated with the angle of repose test. Future research can apply this technique to ultimately calibrate a simulation for powder spreading in the powder bed fusion process.

TABLE OF CONTENTS

LIST OF FIGURES iii

LIST OF TABLES iv

ACKNOWLEDGEMENTS v

Chapter 1 Introduction 1

1.1 Research Goals 7
1.2 Problem Statement 7

Chapter 2 Background Research 8

2.1 Discrete Element Method 8
2.2 Design of Experiments for Simulations 13

Chapter 3 Literature Review 18

3.1 Comparison to Physical Experiments 19
3.2 Decreasing Simulation Time in EDEM 20
3.2.1 Periodic Boundary Conditions 20
3.2.2 Reducing the Particle Shear Modulus 21
3.2.3 Scaling 23

Chapter 4 Methodology 24

4.1 Design of Experiments 24
4.2 Physical Methodology 27
4.3 Simulation Model 29
4.4 Simulation Inputs 32
4.4.1 Creator Tree 32
4.4.2 Simulator 37
4.4.3 Analyst 38

Chapter 5 Results and Discussion 39

5.1 Scaling Runs 39
5.2 Simulation Runs for Particle Interactions 41
5.2.1 Particle to Particle Interaction Runs 42
5.2.2 Particle to Equipment Interaction Runs 47
5.3 Calibration Technique Summarized 52

Chapter 6 Recommendations and Future Work 55

Appendix A Scaling Factors for DEM [30] 57

Appendix B T Value Table [39] 58

BIBLIOGRAPHY 59

LIST OF FIGURES

Figure 1: Process of Powder Bed Fusion [4] 2

Figure 2: Specific Powder Properties [8] 4

Figure 3: Overlapping Particles Defined using DEM [15] 10

Figure 4: DEM Process for Colliding Particles [15] 10

Figure 5: Newton's Equations of Motion [15] 11

Figure 6: Updated Particle Position and Velocity using DEM [15] 12

Figure 7: Representation of Periodic Boundary Conditions [27] 21

Figure 8: Angle of Repose for Various Shear Modulus's [29] 22

Figure 9: How Particle Shear Modulus affects Simulation Time [29] 22

Figure 10: Hall Flowmeter Funnel Dimensions [32] 28

Figure 11: Angle of Repose Pile [35] 28

Figure 12: Full-Scale Angle of Repose Apparatus 30

Figure 13: Front and Side View of the New Model 31

Figure 14: EDEM Creator Tree 32

Figure 15: Bulk Material Inputs in EDEM 33

Figure 16: SEM Image of AlSi10Mg 35

Figure 17: EDEM Simulator Tab 37

Figure 18: EDEM Analyst 38

Figure 19: Particle to Particle Pareto Chart of Standardized Effects 45

Figure 20: Particle to Particle Residual Plots for Effects 46

Figure 21: Particle to Equipment Pareto Chart of Standardized Effects 49

Figure 22: Particle to Equipment Residual Plots for Angle 50

LIST OF TABLES

Table 1: Metrology Methods [9] 5

Table 2: DEM Variables Defined [15] 9

Table 3: Full Factorial 2^4 Design [16] 15

Table 4: Half-Fractional 2^{5-1} Design [16] 16

Table 5: Levels for Each Factor 26

Table 6: Simulation Design of Experiments 27

Table 7: EDEM Bulk Material Variable Inputs 34

Table 8: EDEM Size Distribution Inputs 34

Table 9: Scaled Run Results 39

Table 10: 50.0 Scale Run Results 40

Table 11: T-Test Values 40

Table 12: Factor Variable Definitions 41

Table 13: Particle to Particle Interaction Run Results 43

Table 14: Particle to Particle Main Effects Results 44

Table 15: Particle to Particle Two-Factor Interaction Results 44

Table 16: Particle to Particle Most Accurate Simulation Run 47

Table 17: Particle to Equipment Interaction Run Results 48

Table 18: Particle to Equipment Main Effects Results 49

Table 19: Particle to Equipment Two-Factor Interaction Results 49

Table 20: Particle to Equipment Most Accurate Simulation Runs 51

Table 21: Angle of Repose and Simulation Time based on Shear Modulus and Time Step 52

Table 22: DOE for Simulation 53

ACKNOWLEDGEMENTS

This research and thesis would not have been completed without the help and mentorship of several people. I would first like to thank Sanjay Joshi, my thesis supervisor, for his support and guidance throughout this project. He gave me the opportunity to work in CIMP-3D, I am forever grateful for this experience. Next, I would like to thank master's student Zackary Snow, who has generously assisted me throughout the project and has supported all of my efforts. Thanks for always being there for me. I would also like to thank Catherine Harmonosky for her guidance throughout my undergraduate degree. I would also like to thank Elena Joshi who has generously guided me throughout my studies and research projects during my time at Penn State. A very special thank you goes out to all of my friends and family that have been there for me throughout this journey. Thanks for making the long nights tolerable and for always instilling confidence in me. To my parents, thank you for always believing in me and encouraging me to pursue my dreams. You have made all of this possible for me.

Chapter 1

Introduction

Additive Manufacturing (AM), also known as 3-Dimensional (3D) Printing, is defined as "the process of joining materials to make objects from 3D model data, usually layer upon layer" [1]. This technology has been used to create rapid prototypes for years, but recently has been applied to manufacturing as well. Until recently, most manufacturing fell under subtractive manufacturing where material is removed from an object in order to create the desired shape. Most subtractive manufacturing is done by computer numerical control (CNC) machining, where computers control the machine tools [2]. But subtractive manufacturing can also be as simple as cutting away material from a part [2]. Additive manufacturing is the opposite of subtractive manufacturing where material is repeatedly layered and then fused to create a part. This allows for higher complexity shapes that would otherwise be impossible. However, there are still tasks that are better suited for subtractive manufacturing, most notably ones that require thin, freely moving parts with higher tolerances and surface finishes [2].

There are seven categories of additive manufacturing: VAT polymerization, powder bed fusion, binder jetting, material jetting, sheet lamination, material extrusion, and directed energy deposition [3]. There is also hybrid manufacturing, where a form of directed energy deposition is combined with CNC machining, allowing additive and subtractive manufacturing to be performed using one machine [3]. Powder bed fusion (PBF) is a relatively inexpensive method that offers complexity in its design. This method creates sturdy parts from the strong powder

support structure it creates [4]. There are many advantages of PBF that make it an ideal AM technique, and drives this paper to only focus on PBF.

Before the PBF process can occur, the desired model is created in a Computer Aided Design (CAD) software. Then this 3D model is sliced into thousands of thin layers using a build prep software. These layers are read by the machine software to produce a machine code, which is uploaded into the PBF machine [4]. This code tells the printer exactly what pattern the laser or electron beam needs to follow to melt the particles for each layer. Together, these layers stack to create the 3D model.

In PBF, a thin layer of powder particles is spread across a build plate, most commonly by a roller or a blade. Afterwards a laser or an electron beam fuses the particles into the desired shape based on a 3D model. Once one layer is completed, a new layer of powder particles is spread and fused [4]. The process is repeated until the 3D part is completed. The powder particle material for PBF is either polymers or metal; this paper will only discuss metal PBF. The PBF process is visualized in Figure 1 [4].

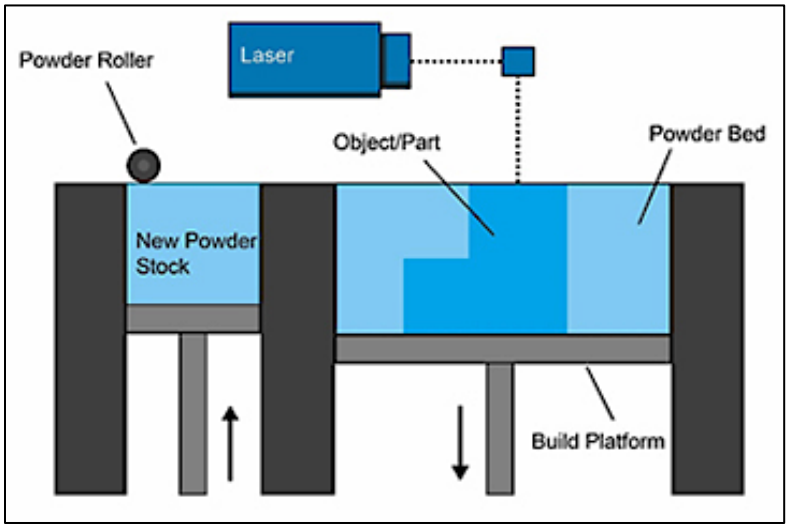

Figure 1: Process of Powder Bed Fusion [4]

PBF is one of the most preferred AM techniques. The layer by layer approach of AM, which PBF performs, enables high geometric complexity and fine resolution in the parts produced. The small powder particle size, usually around 60 microns in diameter, gives a high resolution in the z direction, and the small laser spot, about 50 microns in diameter, gives a good resolution in both the x and y directions [5] [6]. PBF creates extremely sturdy parts due to the small particles packed tightly together and then fused. Lastly, the particles that are not melted can be recycled and reused, creating less waste and making the process cheaper [4].

There are many challenges still present with PBF. For instance, only a few commercial alloys have been developed for AM, limiting the variety of powder that can be used. Additionally, there needs to be more real time process control. “There is a need for real-time, closed-loop process controls and sensor in order to ensure quality, consistency, and reproducibility across AM machines” [7]. Also, the drastic changes in heat often lead to poor heat flow. Poor heat flow can create unwanted microstructures and residual stress buildup, resulting in a distorted part. [7]. Improving the understanding of the process, and the process quality, requires understanding the effect of all the variables beginning with the starting material – the powder that is used to create the layers. Powder characteristics and properties can influence the complete process, and hence it is critical to understand this aspect.

Power properties are broken down into three categories: morphology, chemistry and microstructure. Each is broken down further into the properties that can be measured and calculated, outlined in Figure 2 [8].

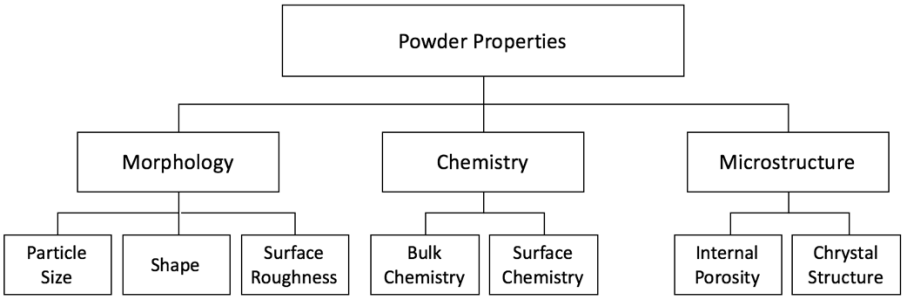

Figure 2: Specific Powder Properties [8]

The morphology of the powder has a significant impact on the final part for powder bed fusion. The particle size, shape, and surface roughness impact how dense the material packs together, the kinetics between the particles when they are melted together, and the final surface roughness of the manufactured part [8]. Without fully understanding the morphology, one cannot understand how the particles will interact with each other during the spreading process and thus predict what the final part will act or look like. For example, unwanted pores can form in parts where the porosity of the powder differs [8]. Although research studies on powder properties exist, there is still no consensus on how the effects of the initial particle characterizations affect the final build part [8]. To understand these power properties, powder characterization tests are performed.

There are several different power characterization methods that are used to measure different powder characteristics. A table of metrology methods and what variables they measure is shown in Table 1 [9].

Table 1: Metrology Methods [9]

Metrology Method	Variables
Helium Psychometry	Particle Density
Laser Diffraction	Particle Size Distribution
X-Rat Computed Tomography	Particle Size and Morphology
X-Ray Diffraction	Particle Crystalline Phases
Scanning Electron Microscopy	Particle Morphology
Energy Dispersion Elemental Analysis	Particle Elemental Composition
X-Ray Photospectroscopy	Particle Surface Molecular/Chemical Composition
Angle of Repose	Particle Density and Morphology

These powder characterization tests are used for measuring certain variables, but they do not capture the complicated processes associated with particle interactions, such as the coefficients that define how particles react when they interact with other particles or equipment. These coefficients are the coefficient of rolling friction, the coefficient of static friction, and the coefficient of restitution. To understand the particles in more depth and the impact of the variables on how the powder particles will behave in use, simulations can be used. Simulating a simple metrology method can help explore certain material properties that the physical test cannot explain. In this thesis, the angle of repose test is simulated because it is a simple test with an easily measured result. This paper focuses on developing a calibration technique that will help understand how certain powder characteristics affect the angle of repose test. The results of this calibration can then be used to calibrate the simulations of spreading in PBF [11].

The angle of repose test is performed by putting a set amount of powder into a funnel that is mounted above a flat surface. This powder is then released from the funnel, allowing it to form a pile on the flat surface. The angle of repose is the measured angle of this conical pile of

powder. This angle can tell a lot about the powder's characteristics, including how the size, shape, density and frictional components combine to affect the angle.

The Discrete Element Method (DEM) is a tool that investigates how particle characteristics and their interactions affect the mechanical behavior of the bulk material [12]. This thesis discusses how the discrete element method is applied to digitally simulate the angle of repose test. EDEM, a commercial software for bulk material simulation, is used. Unfortunately, DEM simulations require a high simulation time due to all the calculations that must be computed. These simulations can take over 24 hours. Scaling of the models is used to accelerate the simulation time, and this thesis explores the effect of scaling on the simulation time as well as its impact on the results.

To calibrate a simulation the simulation result is compared to the physical result. The inputs of the simulation are then adjusted and tested to match the physical test. For this thesis, the physical angle of repose test was performed, and the angle measured. The simulation runs were compared to the physical test result to find the calibrated simulation model. Aluminum power, AlSi10Mg, was used for the experiments in this thesis. AlSi10Mg is a common casting alloy ideal for creating complex geometries. This alloy has specific thermal properties ideal for PBF [11].

1.1 Research Goals

The goal of this thesis is to create calibration techniques for the simulation of DEM models. This calibration technique aims to minimize the amount of time required to calibrate the DEM model, so that future, more advanced simulations can be created. The goal is to have a calibration technique that outlines how to calibrate tests required for powder testing. This calibration will define certain variables that can be calculated and used for other simulations. Ultimately, these calibrations will define all of the EDEM inputs necessary to simulate a full PBF process in EDEM.

1.2 Problem Statement

This thesis aims to develop an efficient method to calibrate a DEM model. DEM models take a long time to calibrate due to the number of calculations that must be computed. Additionally, multiple runs of each DEM simulation must be completed to fully understand the effects of the variables. For the purpose of this thesis, the angle of repose test is chosen as the test method for which the input variables will be calibrated. Aluminum powder (AlSi10Mg) will be used to calibrate this model. The inputs to EDEM required to calibrate the angle of repose test are the coefficient of restitution, the coefficient of static friction, and the coefficient of rolling friction. However, the simulation time step and the particle shear modulus are also analyzed to decrease the simulation time. A design of experiments is proposed to evaluate the effect of the inputs on the angle of repose, while decreasing the number of runs required. This thesis looks at how to decrease the calibration time while ensuring accuracy of the DEM model.

Chapter 2

Background Research

The background research reviewed for this thesis supports the main topics of this thesis, which are discrete element methodology and design of experiments (DOE).

2.1 Discrete Element Method

A big challenge for simulating granular material is understanding the microscopic interactions of the macroscopic particles, like those used in PBF [13]. By understanding these interactions, the material can be better simulated. Luckily, there are physics models that help understand and calculate these microscopic properties to obtain more realistic simulations. The Discrete Element Method (DEM) is an advanced model that predicts how material will deform and react under stress using Newton's laws of motion. DEM evaluates the inter-particle forces of the material based on the overlap, δ, of the particles during collisions in order to understand how they react under stress [14]. All of the variables used in the DEM equations are defined in Table 2.

Table 2: DEM Variables Defined [15]

Variable	Definition
δ	Overlap of particles
r_i	Moment arm of force on particle i
v_i	Initial velocity of particle i
v_i'	Resultant velocity of particle i
F_i	Normal force of collision for particle i
I	Moment of inertia
$\frac{d\omega}{dt}$	Average angular acceleration
M	Rotational motion distance
m	Particle mass
g	Acceleration of gravity
$\frac{dv}{dt}$	Average velocity
F_g	Gravitational force
F_c	Tangential contact force
F_{nc}	Normal contact force
t	Initial time
Δt	Change in time, or time step
$x(t)$	Initial particle position
$x(t+\Delta t)$	Resultant particle position
$v(t)$	Initial particle velocity
$v(t+\Delta t)$	Resultant particle velocity
$a(t)$	Initial particle acceleration
T_R	Time step

For the angle of repose test, the stress develops when particles collide with each other or with equipment. When particles collide, it is modeled as if they have an overlap as shown in Figure 3 [15].

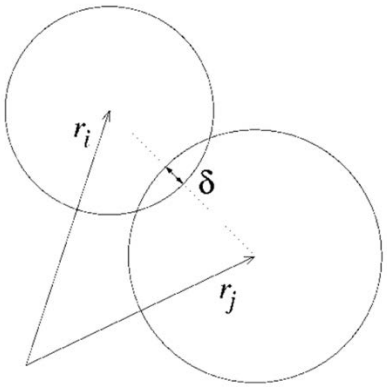

Figure 3: Overlapping Particles Defined using DEM [15]

When particles collide, DEM takes the normal and tangential overlaps and calculates the normal and tangential forces from them. Then it calculates the resultant forces and moments from the collision and uses these forces to solve Newton's equations of motion to get the acceleration. These results calculate the updated velocity and position of each particle [15]. A visual of this process is shown in Figure 4.

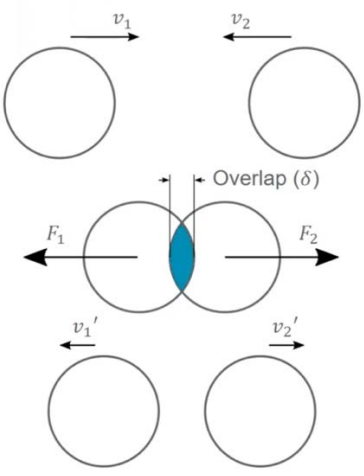

Figure 4: DEM Process for Colliding Particles [15]

Newton's equations of motion, for rotation and translation, dictate the particle's movement. The equation for the rotation of the particle is defined by

$$I\frac{d\omega}{dt} = M \quad [15]$$

Newton's equation for translation is defined by

$$m\frac{dv}{dt} = F_g + F_c + F_{nc} \quad [15]$$

Both of these equations are visualized in Figure 5.

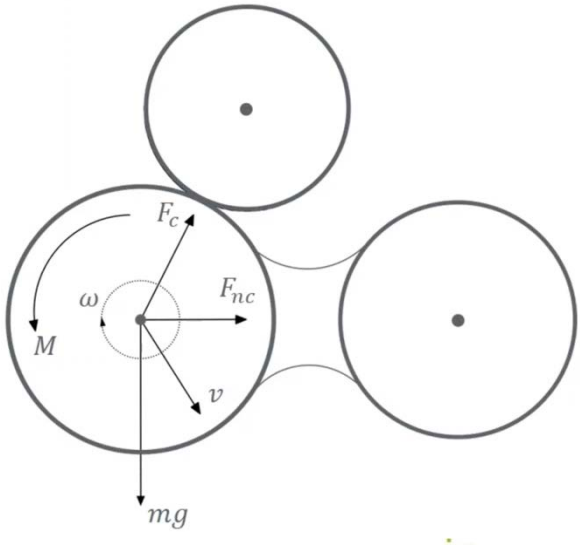

Figure 5: Newton's Equations of Motion [15]

From Newton's equations, the updated particle velocity and position can be calculated for each time step. The new position and the new velocity are defined by

$$x(t + \Delta t) = x(t) + v(t)\Delta t \quad [15]$$

$$v(t + \Delta t) = v(t) + a(t)\Delta t \quad [15]$$

A visual of these changes are shown in Figure 6.

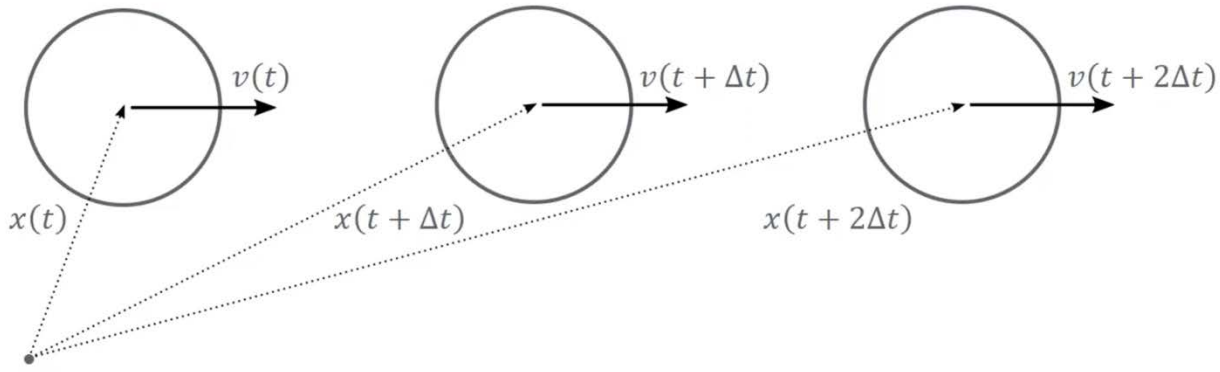

Figure 6: Updated Particle Position and Velocity using DEM [15]

The time step, delta t, defines how much time passes between calculating the updated position and velocity of each particle. The time step has to be extremely small to prevent excessive overlaps and radical movements of the particles [15]. The time step is calculated based on Rayleigh surface waves, which are disturbances from particles far away. The time step must be less than the time it takes for a wave to travel the distance of the smallest particle, T_R [15]. T_R is also known as the theoretical time step. The particle's radius, R, density, ρ, velocity, v, and shear modulus, G are used to calculate T_R.

$$T_R = \frac{\pi R \left(\frac{\rho}{G}\right)^{\frac{1}{2}}}{0.1631v+0.8766} \quad [15]$$

As mentioned, the time step has to be smaller than T_R. To be conservative, normally 20-40% of T_R is used for the time step [15].

2.2 Design of Experiments for Simulations

Experiments are designed to study the effects of several factors, and how they impact the measured response. Each factor can be set to multiple values, or levels, which can either be qualitative or quantitative. In these experiments, known as factorial designs, the effect of a factor is defined by the change in the response produced by the change in the level of that factor [16]. These are called the main effects. When necessary, the interaction effects of factors are also studied. The main effects are how that factor alone affects the response, while the two-factor interactions outline how two factors together affect the response [16]. This continues for three-factor interactions and above.

The Design of Experiments (DOE) for simulations is extremely important to ensure the effects of all inputs are recorded and an accurate analysis of the experiment can be computed. Design of experiments for simulations differ slightly from design of experiments for physical models. In simulations, all inputs, or factors, are controllable, so there is no need for randomness in the experiment [16].

The DOE for simulations is focused on deciding which variables to use as factors and which design is best suited for the model, all while maintaining a reasonable experiment length. Although it is best to have a higher number of variables and a large number of runs to understand all possible interactions, this requires a larger experiment [16].

In many experiments, only two levels are studied for each factor, known as a 2^k Factorial Design with k being the number of factors in the design. This design is often used in early stages of experiments when many factors are being studied. Having only two levels keeps the number of experimental runs down.

A full factorial 2^k design has 2^k runs. For example, to study the effects of four factors, the experiment will have $2^4 = 16$ runs. This design is shown in Table 3. The + signs represent that factor at its high level, and the – signs represent the factor at its low level.

A full factorial design will show all of the main effects, as well as the two-factor and higher interactions. Experimenters can often assume that higher interactions are negligible, they only really care about the main effects and maybe the two-factor interactions. If this is the case, experimenters can run a fractional factorial 2^k design [16].

A fractional factorial 2^k design, 2^{k-q}, where $\frac{1}{2^q}$ is the fraction, is designed to show how the main effects and often the two-factor interactions affect the response, while ignoring the higher order interactions to decrease experimental runs [16]. However, sometimes when designing a fraction-factorial experiment, the effects get confounded with other main effects or interactions. An interaction is confounded if multiple treatments effects are estimated by the same combination of observations [17]. This makes it impossible to tell which interaction actually affected the output. To ensure no desired effects are confounded, the resolution of the design needs to be considered.

A higher resolution means a lower number of assumptions regarding interactions have to be made. The resolution is calculated based on how many interactions are confounded [16]. A full factorial design is said to have resolution “infinity” [17]. Resolution V design are designs where none of the main effects or two-factor interactions are confounded, but two-factor interactions are confounded with three-factor interactions. Resolution IV designs are designs where no main effect is confounded with other main effects or other two-factor interactions, but two-factor interactions are confounded with one another. Resolution III designs are where no

main effects are confounded with one another, but main effects are confounded with two-factor effects [16]. Resolution V design are often used to efficiently understand main and two-factor interaction effects, but sometimes lower resolutions must be used due to resource constraints.

For a 5-factor experiment, a full factorial design, 2^5, has 32 runs. Depending on the experiment, this may be too many runs. A half-fractional design, 2^{5-1}, only has 16 runs without confounding any of the two-factor interactions. Completing a 2^{5-1} experiment gives a resolution V design, allowing the experimenter to understand the main effects and the two-factor interactions but not the higher resolution effects. Again, for many experiments this is sufficient information.

A half-fractional design is set up the same way as the full factorial design for the experiment with one less factor. Then a column is added for the final factor. To calculate the level for this factor, multiply all levels in the first k-1 columns. An example of this process for the 2^{5-1} design is shown in Table 3 and Table 4 [16].

Table 3: Full Factorial 2^4 Design [16]

Runs	Factor 1	Factor 2	Factor 3	Factor 4
1	+	+	+	+
2	-	+	+	+
3	+	-	+	+
4	-	-	+	+
5	+	+	-	+
6	-	+	-	+
7	+	-	-	+
8	-	-	-	+
9	+	+	+	-
10	-	+	+	-
11	+	-	+	-
12	-	-	+	-
13	+	+	-	-
14	-	+	-	-
15	+	-	-	-
16	-	-	-	-

Table 4: Half-Fractional 2^{5-1} Design [16]

Runs	Factor 1	Factor 2	Factor 3	Factor 4	Factor 5
1	+	+	+	+	+
2	-	+	+	+	-
3	+	-	+	+	-
4	-	-	+	+	+
5	+	+	-	+	+
6	-	+	-	+	+
7	+	-	-	+	+
8	-	-	-	+	-
9	+	+	+	-	-
10	-	+	+	-	+
11	+	-	+	-	+
12	-	-	+	-	-
13	+	+	-	-	+
14	-	+	-	-	-
15	+	-	-	-	-
16	-	-	-	-	+

A 2^k factorial design assumes linearity by only testing each factor at two levels, meaning this design only tests the linear effects of the model, and not the quadratic or higher effects. Although the 2^k design still works well when it is only approximately linear, many experimenters want to test and understand the quadratic effects as well. Adding center point runs to an experiment will test the curvature of the model and prove if quadratic effects exist [16]. A center point run is a run at the center point of each factor. The center point of each factor is the average of the factor's two levels. If multiple center point runs are performed, an independent estimation of error can be calculated [16]. An independent estimation of error means that the error is calculated from uncorrelated sources. In this scenario these are the identical center point replications [18]. This is another downfall to the 2^k design that is resolved with center point runs.

A central composite design is performed if the designed is believed to fit a quadratic model [19]. If a center-point DOE is run and quadratic effects are present in the model, then a central composite design can be performed to understand these effects [16]. The model is this thesis is not believed to fit a quadratic model because only the main effects are predicted to significantly affect the angle of repose, not the combination of the main effects.

Chapter 3

Literature Review

There have been multiple papers published regarding how to calibrate and validate DEM models, some even targeting the angle of repose test.

The literature review shows that the current way to calibrate DEM models is by comparing the results of the model to the results of physical tests, then adjusting the inputs of the model until calibration is achieved [20]. Due to the ease and availability of resources, most papers only compare the end result of both and not the other variables that contribute to this result. For example, some papers only compare the resultant angle of repose measurement and not the powder characteristics that affect it. However, some papers have compared the resulted calibrated input values to the known powder characteristics [21]. This requires knowing these powder characteristics for the physical powder, such as the coefficient of restitution, which is often unknown due to equipment limitations [21].

Literature on efficiently calibrating the model was also reviewed. DEM is often time consuming due to the large number of calculations required. Because of this, recent literature has focused on how to decrease calibration time while ensuring accuracy. Calibration time can be decreased by either decreasing the simulation time or decreasing the total number of simulations required. Even with this research, accurate calibration methods are often questioned on the validity of the measured parameters from the simulations [22].

3.1 Comparison to Physical Experiments

The first step to any calibration technique is to run the physical tests and measure the characteristics that can be measured. Ideally, every characteristic of the powder would be physically tested to get a full understanding of the material. However, this requires a significant amount of time and resources to accomplish. Depending on the equipment and resources available, different characteristics will be measured using various calibrations. Grim and Wypych [22] were able to measure the coefficient of restitution of their coal powder by taking a picture of the falling powder using a high-speed camera. Single property laboratory tests can also be performed to understand a specific property of the powder [21]. For example, a particle sliding test can be done to determine the coefficient of static friction [21]. While performing separate tests to measure specific physical characteristics of the powder leads to a more validated model, it is not required to produce an accurate simulation [23]. These tests are extremely time consuming and require certain apparatuses that are not always available. For this, most calibration techniques published only compare one measurement, such as the angle of repose. This one measurement can then be used to explain other powder characteristics, such as the coefficient of restitution and the coefficient of static friction [20] [24].

The published calibration techniques lack a clear method for comparing the simulation to the physical test. Many just compare the results and adjust the simulation according to their knowledge of how the inputs affect the output [23]. For example, Wuist and Evertsson [21] graphed all of the input combinations and the resultant output each simulation gave. From these graphs, they analyzed trends to predict what combination of inputs provides an accurate output. This method can only look at one variable at a time, as opposed to a factorial design. Although

this is a thorough and practical way to calibrate the inputs, certain interactions may be missed. For instance, this graph does not show the two-factor interaction effects which may have significant effect on the output [21].

3.2 Decreasing Simulation Time in EDEM

Several methods are used in DEM to reduce simulation time. Techniques often discussed in literature include adding periodic boundary conditions, reducing the particle shear modulus, and most significantly, scaling the entire simulation. Decreasing the calibration time can be achieved by reducing the simulation time, or by decreasing the number of simulations run.

3.2.1 Periodic Boundary Conditions

In order to obtain a realistic view of the model in most simulation applications, the system is treated like a bulk environment. Periodic boundary conditions dictate what happens to the particle once it leaves the simulation domain, achieving this bulk behavior for the system [25]. In EDEM, periodic boundaries can be set for any or all of the axes. When an axis is selected, if a particle leaves the simulation domain in that direction, it will re-enter on the opposite side [26]. Periodic boundary conditions allow the user to choose a smaller simulation environment, most commonly a thin cross-section of the model, while eliminating the need to generate a large number of particles. A two-dimensional representation of periodic boundary conditions is shown in Figure 7. If any of the particles in the center simulation cell exit, they will

immediately be replaced by a particle from the cell opposite to where it exited, keeping the total number of particles in the center cell constant [26].

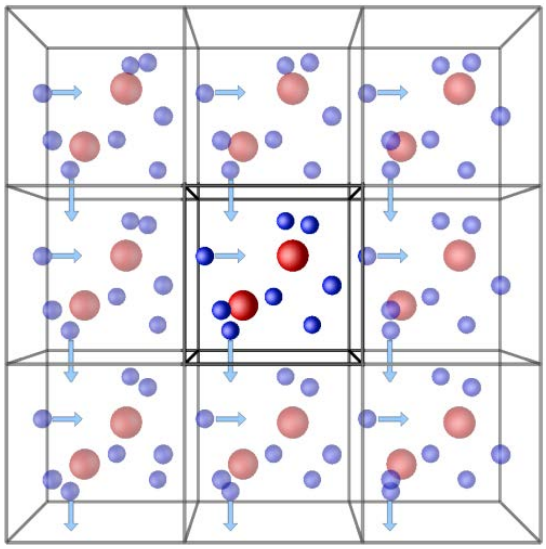

Figure 7: Representation of Periodic Boundary Conditions [27]

3.2.2 Reducing the Particle Shear Modulus

The particle shear modulus is an elastic coefficient of the particle, describing how the particle deforms and responds when interacting with another surface [28]. Previous research has shown that reducing the particle shear modulus in a simulation can significantly reduce the time necessary to run the simulation without changing how the particles interact with one another. As discussed in Section 2.1, the shear modulus is needed to calculate T_R. The higher the T_R is the higher the time step can be, leading to a lower simulation time. The time step equation proves that a lower shear modulus leads to a higher T_R, and thus a lower simulation time.

Cole [29] specifically tested this using the angle of repose test in EDEM. The results showed that above a shear modulus of 1×10^6 Pa the behavior of the bulk material does not significantly change, resulting in very similar angles of repose, shown in Figure 8 [29].

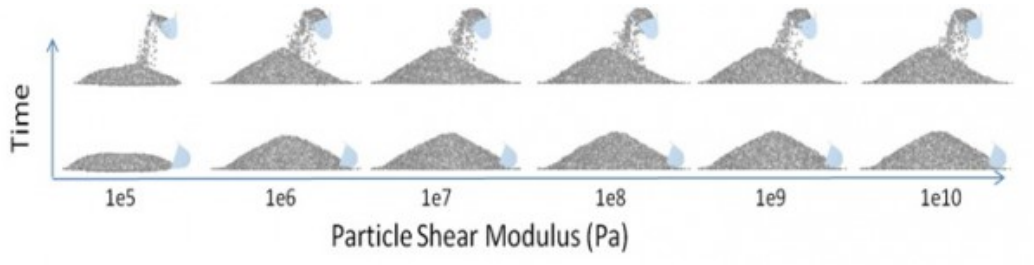

Figure 8: Angle of Repose for Various Shear Modulus's [29]

Cole [29] also showed that while the angle of repose does not change, the simulation time notably decreases. The graph in Figure 9 shows that every reduction in shear modulus by a factor of 100 results in a 10 times faster simulation [29].

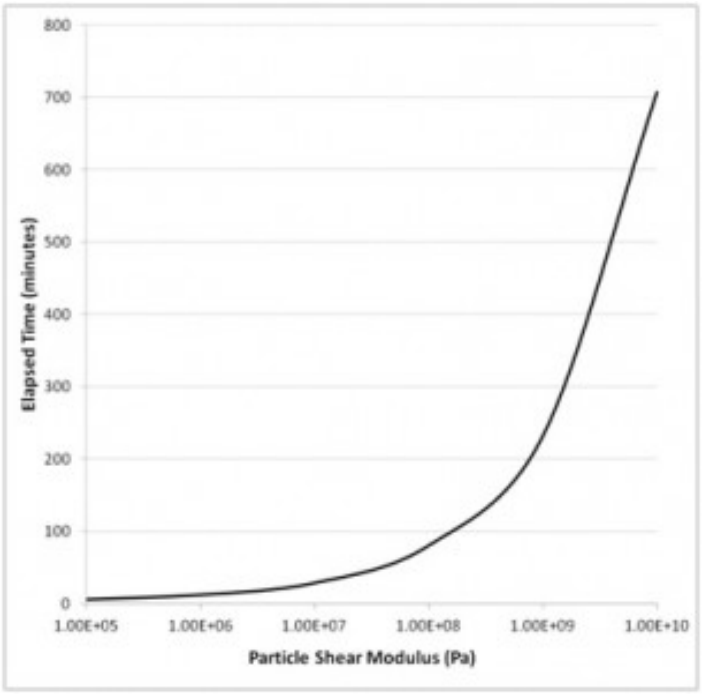

Figure 9: How Particle Shear Modulus affects Simulation Time [29]

3.2.3 Scaling

Scaling is often used in simulations to reduce the required simulation time while maintaining the accuracy of the results. To scale a simulation, several variables must be scaled correctly to ensure scale-invariant properties and particle interactions. Scale invariance means that no feature of an object is changed when the particle is scaled. All properties must be scale invariant in order to understand the interaction laws for a scaled model. For this, each variable cannot be independently scaled. The interaction laws are scaled first and then used to understand which variables need to be scaled to obtain full scale-invariance in the model. Feng and Owen [30] outline all of the necessary scaling relationships for DEM, which and are shown in Appendix A.

For the angle of repose simulation, the particle's radius and the physical measurements of the equipment need to be scaled. All of these scales are linear, meaning the constant scaling factor decided on, h, must be multiplied by each full-scale dimension to obtain a correctly scaled model [30].

Chapter 4

Methodology

This section details how the research for this thesis was conducted, including the DOE created, the physical methodology required to perform the angle of repose test, how the simulation model was created, and what simulation inputs are required. The DOE approach was completed to ensure the effects of the input variables on the output could be understood, while reducing the required number of simulation runs to decrease calibration time [15].

4.1 Design of Experiments

The angle of repose is defined by several variables. While most of these variables can be directly measured, some are currently very difficult to measure. Three variables that are extremely tough to measure are: the coefficient of restitution, the coefficient of rolling friction, and the coefficient of static friction. These three variables will be inputs in the DOE. However, the goal of the model is to get an accurate angle of repose measurement while reducing the simulation time to decrease the overall calibration time. Because of this, the shear modulus and the percent of T_R, the theoretical time step, are also input variables for this DOE.

A full design would have eight factors: three coefficients for the particle to particle interaction, three for the particle to equipment interaction, one for the shear modulus, and one for the time step. This would lead to a 256 run full factorial design, and even a 128 run half factorial design. Both designs require too many runs to be feasible.

As discussed in Section 4.2, the angle of repose is measured at the top of the pile, meaning the particle to particle interactions dictate the measured angle. To get a realistic looking simulation, the particle to equipment interactions are also important. In order to reduce the DOE and calibration time, two separate design of experiments will be performed: one to understand the coefficients for the particle to particle interaction and one to understand the coefficients for the particle to equipment interaction. These designs require five inputs: the three coefficients, the shear modulus, and the time step.

Since the particle to particle interactions dictate the angle, the particle to particle DOE will be conducted first. This experiment will have the particle to equipment coefficients at their maximum values, the largest friction, for control because it was observed that the physical particle to equipment interactions occur with a high frictional coefficient. The angle of repose from each simulation run will be compared to the physical angle of repose to find the ideal values for the inputs. Then the particle to equipment DOE will be conducted with the particle to particle coefficients set at these ideal values.

A 2^k design was chosen for both experiments to understand the linear effects of the model. It is assumed that two levels for each factor is suitable and will reduce the number of runs. The levels for each factor are outlined in Table 5. The known shear modulus from the powder is 2.65×10^{10} pascals, which was set as the high level to test if decreasing the shear modulus could decrease the simulation time while still accurately simulating the angle of repose. The low level for the shear modulus, and the levels for the time step were decided based on literature review discussed in Section 3.2.2. The values for the coefficient of restitution and coefficient of static friction can range from 0 to 1. Preliminary simulation runs proved that the levels should be set at 0.1 and 0.9 to capture the full effect of these factors [5]. The levels for the

coefficient of rolling friction are known to range from 0 to 0.2 for AlSi10Mg [11]. The preliminary runs also suggested setting this value close to its limits to capture the full effect of the factors [5]. These levels are for both the particle to particle interaction and the particle to equipment interaction.

Table 5: Levels for Each Factor

	Low Level (-)	Center Point (0)	High Level (+)
Shear Modulus (pascals)	2.65×10^6	2.65×10^8	2.65×10^{10}
Coefficient of Restitution	0.1	0.5	0.9
Coefficient of Static Friction	0.1	0.5	0.9
Coefficient of Rolling Friction	0.05	0.1225	0.195
Time Step	20%	50%	80%

A 2^5 full factorial design has 32 runs, requiring a total of 64 runs for both interactions. This experiment would take about two months to perform. However, a half fractional 2^{5-1} design only requires 16 runs, meaning 32 runs total, a feasible number of runs. This design is suitable for this experiment assuming that only the main effects and the two factor effects are significant. Four center point runs were added to this design to achieve an independent estimation of error. The full design for both experiments is shown in Table 6. The + signs represent that factor at its high level, the – signs at its low level, and the 0 at its center point. Every run was simulated, and both the angle of repose and the simulation time were measured.

Table 6: Simulation Design of Experiments

Run #	Shear Modulus	Coefficient of Restitution	Coefficient of Static Friction	Coefficient of Rolling Friction	Time Step
1	-	-	-	-	-
2	+	+	-	-	-
3	+	-	+	-	-
4	-	+	+	-	-
5	+	-	-	+	-
6	-	+	-	+	-
7	-	-	+	+	-
8	+	+	+	+	-
9	+	-	-	-	+
10	-	+	-	-	+
11	-	-	+	-	+
12	+	+	+	-	+
13	-	-	-	+	+
14	+	+	-	+	+
15	+	-	+	+	+
16	-	+	+	+	+
17	0	0	0	0	0
18	0	0	0	0	0
19	0	0	0	0	0
20	0	0	0	0	0

4.2 Physical Methodology

The angle of repose test is one of the simplest and most widely used powder characterization tests. The test is performed following ASTM Standard C1444 [31]. The test is executed by putting a specific amount of selected metal powder, 50 grams for this thesis, into a funnel that is mounted in a stand with the powder outlet 75 mm above the flat surface, also called a base plate. For this thesis, the Hall Flowmeter Funnel was used. The ASTM standards for the dimensions of the Hall Flowmeter Funnel are shown in Figure 10 [32]. The standard equipment material is brass, which was used for the experiments in this thesis.

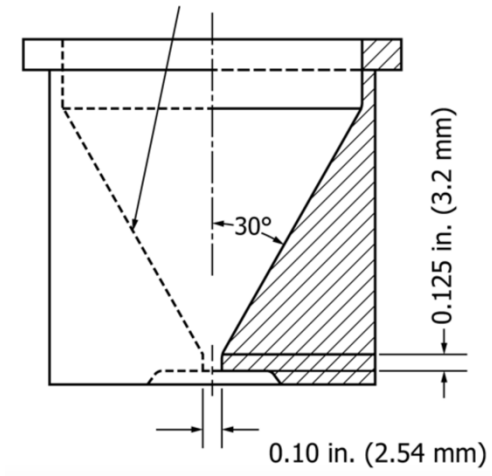

Figure 10: Hall Flowmeter Funnel Dimensions [32]

The powder is then released from the funnel, falls, and piles itself onto the base plate. The angle of repose is the measured angle of the conical pile of powder that forms on the flat surface. It can also be calculated using an equation where α is the angle of repose, h is the height of the pile, and D is the diameter of the base of the powder cone [33].

$$\tan(\alpha) = \frac{2h}{D} \quad [33]$$

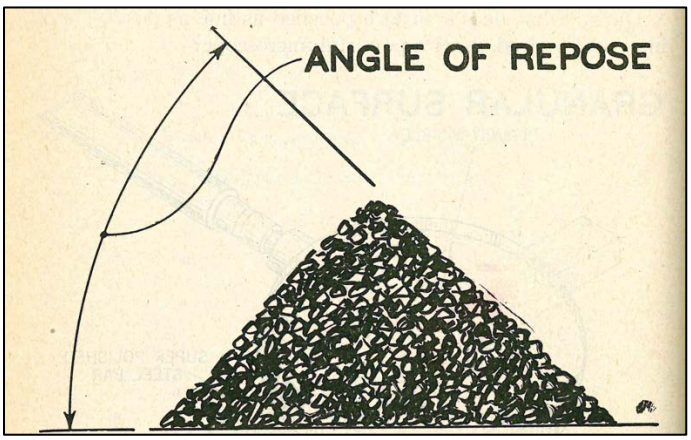

Figure 11: Angle of Repose Pile [35]

A visual of the angle of repose is shown in Figure 11. This angle can explain how certain powder characteristics, such as the size, shape, density and frictional components, combine to affect the angle.

Every time particles interact with other particles or the equipment, inter-particle forces are present. These forces dictate how the particles react to these interactions. When particles fall and make contact with either the equipment or the particle pile, they slide and roll until the frictional force is large enough to overcome the gravitational force acting along the angle of inclination [33]. How the particles slide and roll off of each other is dictated by the inter-particle forces. All of the forces balance out to form the final angle of repose. The angle of repose will be high if the cohesion of the powder if high, and low if not.

4.3 Simulation Model

The majority of the work for this thesis was done to set up the simulation model in EDEM. In the beginning the full-scale angle of repose apparatus was designed in SolidWorks, a computer-aided design modeling software, and then imported into EDEM. This is shown in Figure 12.

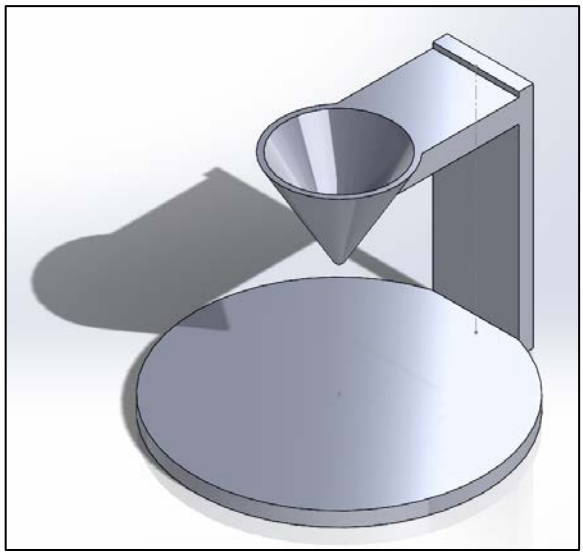

Figure 12: Full-Scale Angle of Repose Apparatus

The simulation was setup and run, but after 50 hours it still was not completed. This simulation time was extremely large due to the extremely small particles, as well as the large 75 mm drop required for the particles, creating an infeasible experiment.

The next model created aimed to fix one of these problems by scaling up the equipment and the particles. With a scale as large as 100, the simulation time was still too high, at about 16 hours, due to the 75 mm drop required before the particles even started forming an angle on the build plate.

From this, a completely new model was created. This model does not physically emulate the angle of repose test, but it still mirrors the physics of the angle of repose test. The new model contains a rectangular “funnel”, where all of the particles are generated, and a “base” where all the particles fall and pile on to once all the particles are generated and released from the “funnel”. The cross-sectional view of this model is similar to the cross-sectional view of the actual angle of repose test, excluding the shape of the funnel. However, other views show the

main two differences. The new model has only a 10 mm drop, compared to the old 75 mm drop, and a cross-sectional width of only 15mm. This width drastically reduces the simulation time, while still maintaining an accurate cross-sectional view of the simulation [34]. Screenshots of this model are shown in Figure 13.

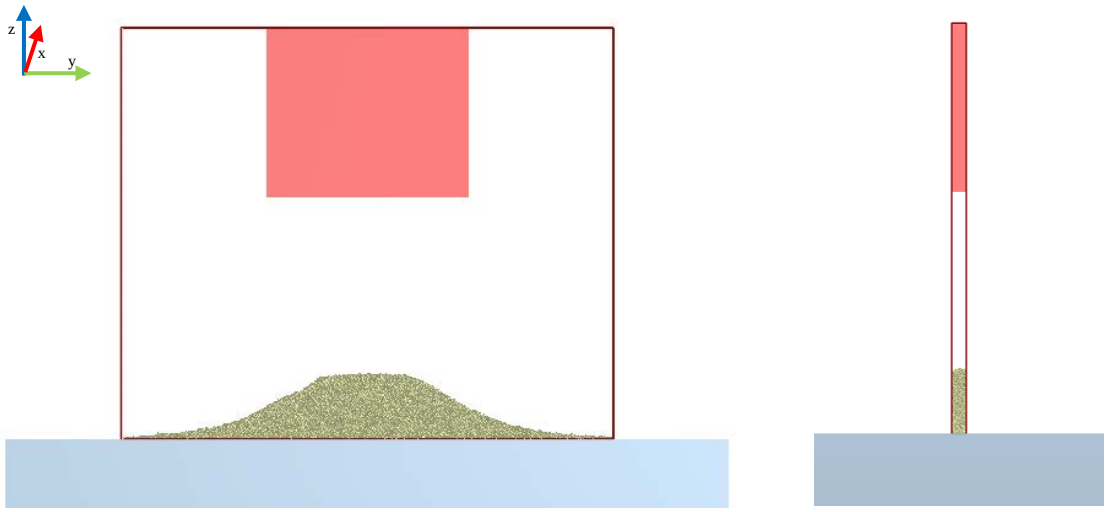

Figure 13: Front and Side View of the New Model

This new simulation, ran at full scale, reduced simulation time to about 14 hours, which is still too high considering the number of runs that need to be performed. To decrease simulation time more, scaling was introduced. The larger the model is scaled, the lower the simulation time will be. However, too high of a scale may produce unrealistic results. The model was run at full-scale, 10.0 scale, 25.0 scale, and 50.0 scale. To test precision of the model, a t-test with 95% confidence was performed to test if the scaled angle was different than the full-scale angle. This tested to discover which scale, if any, could be used for the entirety of the experiment. The results of this t-test in Chapter 5 and prove that a 50.0 scaled model can be used for the entirety of this thesis.

4.4 Simulation Inputs

Once the simulation model is imported into EDEM, several variables must be calculated and set in order for the simulation to mimic the physical test. EDEM is broken into three sections: Creator Tree, Simulator, and Analyst.

4.4.1 Creator Tree

The Creator Tree is where all of the variables are defined for the model, divided into the ones for the bulk material, equipment material, geometries, physics, and environment. A screenshot of the Creator Tree is shown in Figure 14.

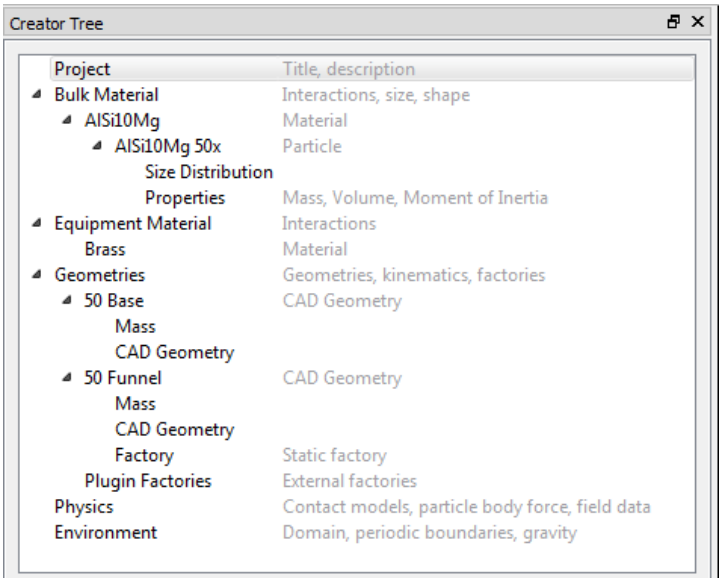

Figure 14: EDEM Creator Tree

In both the bulk and equipment material subsections, the specific bulk materials being used must first be defined. This requires inputting Poisson's ratio (v), solids density (ρ), and either shear modulus (G) or Young's modulus (E). Both the particle to particle and the particle to

equipment interaction must be defined. These interactions require defining the coefficient of restitution, the coefficient of static friction, and the coefficient of rolling friction.

Each simulation can have many different types of materials. Because of this, the particle ratios for each bulk material must be defined. The particle ratio is the ratio of powder in the experiment that consists of that bulk material. This experiment only has one powder, so the particle ratio is 1. A screenshot of this input screen is shown in Figure 15.

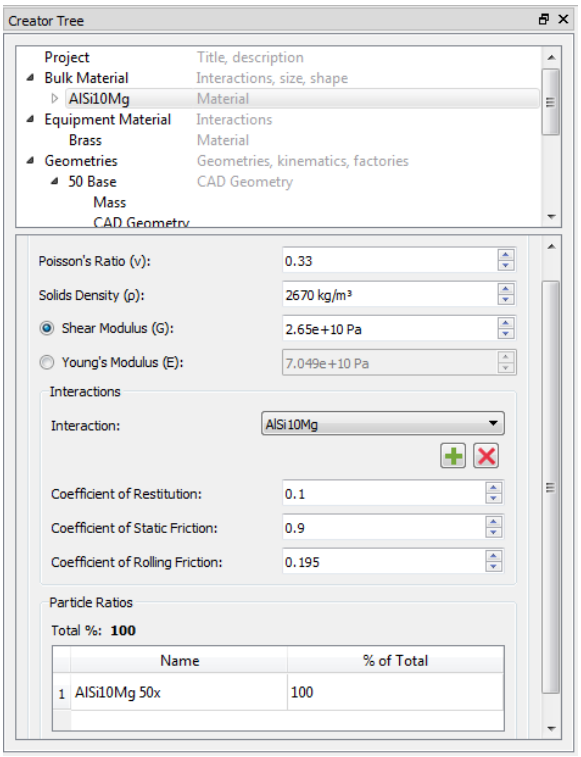

Figure 15: Bulk Material Inputs in EDEM

AlSi10Mg is the bulk material used, and brass is the equipment material used for all simulations and experiments for this thesis. The values of the inputs for both materials are outlined in Table 7. The * represents those variables that were tested in the design of experiments outlined in sections 3.4 and 3.5, so their values changed depending on the DOE.

Table 7: EDEM Bulk Material Variable Inputs

Variable	Bulk Material Value	Equipment Material Value
Poisson's Ratio (v)	0.33	0.34
Solids Density (ρ)	2670 kg/m^3	8490 kg/m^3
Shear Modulus (G)	*	1.3×10^{10}
Coefficient of Restitution	*	*
Coefficient of Static Friction	*	*
Coefficient of Rolling Friction	*	*
Particle Ratios	100% of total	

After defining the bulk material, the size distribution of the particles must be described. This requires selecting a certain size distribution, specifying how it is scaled, inputting the mean and standard deviation of that distribution, and inputting the physical radius. The size distribution inputs for the model used in this thesis are outlined in Table 8. This is known information based on the powder being used.

Table 8: EDEM Size Distribution Inputs

Variable	Value
Size Distribution	Lognormal
Scaled	Linear by volume
Mean	1
Standard Deviation	0.50
Physical Radius (50.0 scale)	1.92 mm

The mass, volume, and moment of inertia, also known as the powder properties in EDEM, are the last variables to define for the bulk material. EDEM can calculate these properties based on spheres, manual, or an imported template. The AlSi10Mg properties are calculated based on spheres in this thesis because AlSi10Mg has extremely sphere-like particles, as shown in Figure 16. This picture was taken in previous research using a scanning electron

microscope (SEM). From here, EDEM can automatically center the particle, and calculate its properties, which was done for this model.

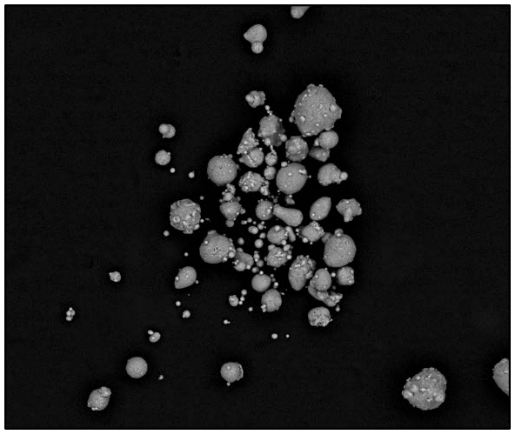

Figure 16: SEM Image of AlSi10Mg

In the geometries subsection the CAD models get imported. After import, their equipment material must be specified and whether the geometry is physical or virtual. For this model, only two geometries were necessary, the funnel and the base. Since brass was the only equipment material defined, every geometry was automatically set to brass. The funnel began as a physical geometry, so the particles could be contained within the funnel. After all particles were generated, the funnel was switched to a virtual geometry, allowing all particles to free fall onto the base. The base remained physical the entire time so that the particles could fall onto it.

In the geometries subsection the center of mass, and the rotation, translation, and distance of the CAD geometry must be defined. This can be automatically calculated based on the imported CAD geometry and requires no additional inputs.

For the physics subsection, the contact models for the interactions must be defined. Contact models describe how elements behave when they come in contact with other elements. The most simplified contact model is a linear contact model, which discusses the linear relationship between force and displacement [36]. This model assumes that the strain in the

material is small, stress and strain are proportional, the material returns to its initial shape after deformation, and there is not dependence on loading or straining [37]. A popular non-linear contact model is the Hertz-Mindlin model. This model was developed to understand the contact behavior for spherical shapes [36]. This model is broken down into normal contacts, shear interactions, and tangential or rolling friction interactions. A spring-dashpot response is used to describe normal contact, a frictional coefficient describes the shear interactions, and another spring-dashpot response describes the tangential or rolling friction interaction [38]. These contact forces are calculated based on equations of motion [36]. A basic Hertz-Mindlin contact model was used for both particle to particle, and particle to equipment interactions in this calibration. For a more in depth understanding of various contact models, refer to Peng's paper "Discrete Element Method (DEM) Contact Models Applied to Pavement Simulation" [36].

The environment subsection is where the domain, periodic boundaries, and the gravity is defined. The domain is the only area of the model that is simulated. Nothing outside of the set domain will be modeled. To reduce simulation time, this domain can be set to a smaller area. The domain for this model is only around the funnel when particles are being generated. Once all particles are generated and the funnel is turned to virtual, the particles begin to fall. At this point the domain is expanded to include the base. Because this simulates a real-world experiment, gravity is defined in the Y direction as -9.81 m/s^2. The periodic boundaries are set in the X direction for this model, allowing particles that exit the domain in the X direction and re-enter on the opposite side.

4.4.2 Simulator

The simulator tab is where to define how the simulation will run. Most inputs are automatically calculated based on particle size, but some still need to be manually inputted, including the time step, simulation time, and the target save interval. The time step is the amount of time between each calculation in the simulation and directly impacts the simulation time [26]. The simulation time is the length of real time the simulation represents. For this model, the simulation time was set to one second, allowing all of the particles to fall and settle into the angle of repose. Lastly, the target save interval defines how frequently the model is saved. At any point the model can be paused and returned to any target save interval to view the simulation at that time. Too high of an interval may withhold certain data from being seen, and too low of an interval will lead to extremely large files and slightly higher simulation times [26]. A target save interval of 0.01 seconds was used for this model. A screenshot of the simulator table is in Figure 17.

Figure 17: EDEM Simulator Tab

4.4.3 Analyst

The analyst tab shown in Figure 18 is where to view and analyze the simulation once it is completed. This allows the user to view and export their simulation at every saved time interval, which all can be put together to form a video if desired. The analyst pane also allows users to use certain tools to analyze their simulation, such as a ruler or protractor. For the model in this thesis, the analyst tab was used to view the full simulation and export the final angle of repose simulation image. Once the final simulation image was exported and saved, ImageJ software was used to measure the angle of repose from the picture. This angle was measured 5 times, and the angle recorded is the average of these measurements in order to reduce error.

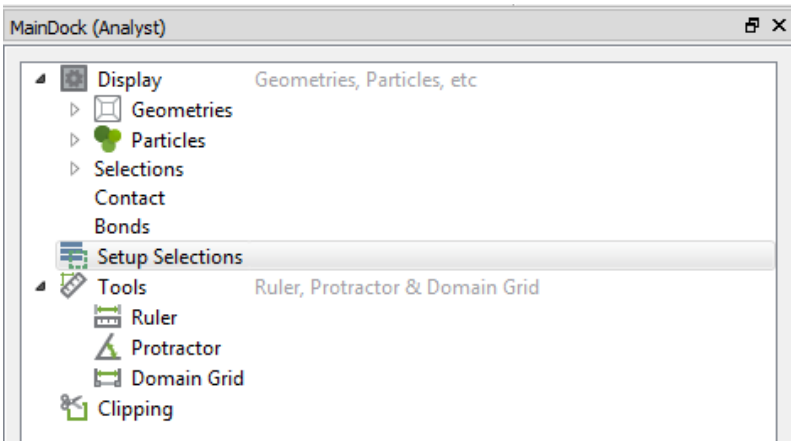

Figure 18: EDEM Analyst

Chapter 5

Results and Discussion

5.1 Scaling Runs

The simulation was run at full-scale, 10.0 scale, 20.0 scale, and 50.0 scale. The results, outlined in Table 9, show that the angle of repose measured at each scale is similar, with a maximum of 2° difference, while the simulation times vary.

Table 9: Scaled Run Results

Scale	Angle of Repose (°)	Simulation Time (hours)
1.0	22.0	80
10.0	20.0	35
25.0	22.5	14
50.0	21.7	4

A t-test with 95% confidence was performed to test if there is statistical significance in the scaled angle simulation verse the full-scaled angle simulation. This tested precision of the simulation, not accuracy to the physical simulation. This did not test accuracy because the known input values are only going to be understood after the design of experiments is complete. This is why this t-test compared the resulted angle to 22.0°, the angle of the full-scale simulation. Since all scaled angles were similar, the 50.0 scale was tested for significance first, because this resulted in the lowest simulation time. A t-test was performed because the population standard deviation is unknown, and the 50.0 scale model was run only 6 times. The test was performed in Minitab. To test statistical significance, the angle measured from the six 50.0 scale simulations,

outlined in Table 10, were compared to the angle measured from the full-scale run, 22.00°. A new bed of powder was created for each simulation based on the radius and size distribution input into EDEM. This distribution leads to a slightly different pack of powders each time, resulting in slightly different simulations and results.

Table 10: 50.0 Scale Run Results

Run #	Angle of Repose (°)
1	21.67
2	22.17
3	21.88
4	22.00
5	21.67
6	21.88

The null and alternative hypothesis for this t-test where θ_{50} is the angle of the 50.0 scale model are below.

$$H_0: \theta_{50} = 22.0^\circ$$

$$H_1: \theta_{50} \neq 22.0^\circ$$

The two-sided t-test with 95% confidence is outlined below.

Table 11: T-Test Values

α	0.05
n	6
$\bar{X}_\theta$	21.878
s_θ	0.1932

$$t\ score: t = \left| \frac{\bar{X} - 22.0}{S/\sqrt{n}} \right|$$

$$t = 1.547$$

$$p\ value \approx 0.20$$

A t-value table was used to find the p-value associated with this t-score. A t-value table is attached in Appendix B. A t-score of 1.547 with 6 samples yields a p-value of approximately 0.20 [39]. This p-value is larger than the α value of 0.05, so the null hypothesis cannot be rejected. This means the 50.0 scale angle is not statistically different than the full-scale angle. Due to this, the 50.0 scale simulation is used for the entire DOE for this thesis.

5.2 Simulation Runs for Particle Interactions

Minitab was used to analyze the results of the simulation runs for the particle to particle interactions, and the particle to equipment interactions. All of these runs were run with a 95% confidence. There are three degrees of freedom due to the four center point runs. For simplicity, the following variables are used to represent each of the factors in this section.

Table 12: Factor Variable Definitions

Factor	Variable
Shear Modulus	X_1
Coefficient of Restitution	X_2
Coefficient of Static Friction	X_3
Coefficient of Rolling Friction	X_4
Time Step	X_5

5.2.1 Particle to Particle Interaction Runs

The results of all particle to particle interactions runs are in Table 13. The last four runs are the center point runs. Each angle was measured five times then averaged to get an accurate measurement. The estimated time it took the simulation to run is also outlined in the table. This time is an estimation because the simulation time EDEM outputs is independent of the computational power available from the computer at that time. The real time it took the simulation to run depends on how powerful the computer is and what other programs are running. In this experiment, two runs failed to simulate, represented as '---' in the table. Both of these runs had a low shear modulus and a high time step. The other two runs with a low shear modulus and a high time step simulated erratically, leaving no angle to measure. This is represented as 00.0° in the table. These results prove that this combination of input levels cannot be simulated correctly using this software. The high time step allows for the particles to travel further and interact more before the particle interactions are calculated again. This often leads to erratic behavior for the particles [15]. A low shear modulus means the particles are more flexible, leading to a large displacement after collision [15]. A combination of these effects results in the particles traveling a significant distance after one collision, which is hard to calculate and understand in DEM [15]. This is an example of one of the limits of the software that must be considered and understood to calibrate it correctly.

Table 13: Particle to Particle Interaction Run Results

Run #	Angle of Repose	Estimated Simulation Time (minutes)
1	11.0°	9
2	19.0°	250
3	26.0°	290
4	25.0°	18
5	19.0°	260
6	17.6°	12
7	15.0°	17
8	39.7°	310
9	19.0°	115
10	00.0°	2
11	---	---
12	27.0°	140
13	---	---
14	19.0°	120
15	29.9°	130
16	00.0°	1
17	27.4°	18
18	28.6°	18
19	26.1°	20
20	27.2°	21

An analysis of variance test with 95% confidence was completed for the angles from this data. This test tests each main effect and interaction effect to see if it significantly affects the angle of repose. The null and alternative hypothesis are below.

H_0: X_i or X_i X_j does not affect the angle of repose

H_1: X_i or X_i X_j affects the angle of repose

For the analysis of variance, the factors and interactions with a p-value below 0.05 mean they significantly influence the angle of repose. The results show that all of the main factors and most of the two-factor interactions are significant, outlined in Table 14 and Table 15.

Table 14: Particle to Particle Main Effects Results

Factor	P-Value	Significant?
X_1	0.027	Yes
X_2	0.001	Yes
X_3	0.003	Yes
X_4	0.037	Yes
X_5	0.003	Yes

Table 15: Particle to Particle Two-Factor Interaction Results

Interaction	P-Value	Significant?
$X_1 * X_2$	0.000	Yes
$X_1 * X_3$	0.005	Yes
$X_1 * X_4$	0.115	No
$X_1 * X_5$	0.002	Yes
$X_2 * X_3$	0.033	Yes
$X_2 * X_4$	0.179	No
$X_2 * X_5$	0.000	Yes
$X_3 * X_4$	0.000	Yes
$X_3 * X_5$	0.017	Yes

The Pareto Chart in Figure 19 displays the absolute values of the standardized effects. The standardized effects are the t-test statistics that test if the null hypothesis is true. The red reference line is the t-test statistic with 95% confidence and three degrees of freedom, which is 3.18 [39]. The Pareto chart visualizes the magnitude and importance of each effect. The effects that cross the reference line have a t-test statistic above 3.18, meaning their p-value is below 0.05. The more the effect crosses that reference line, the more significant it is [40]. This backs up the data in Tables 14 and 15.

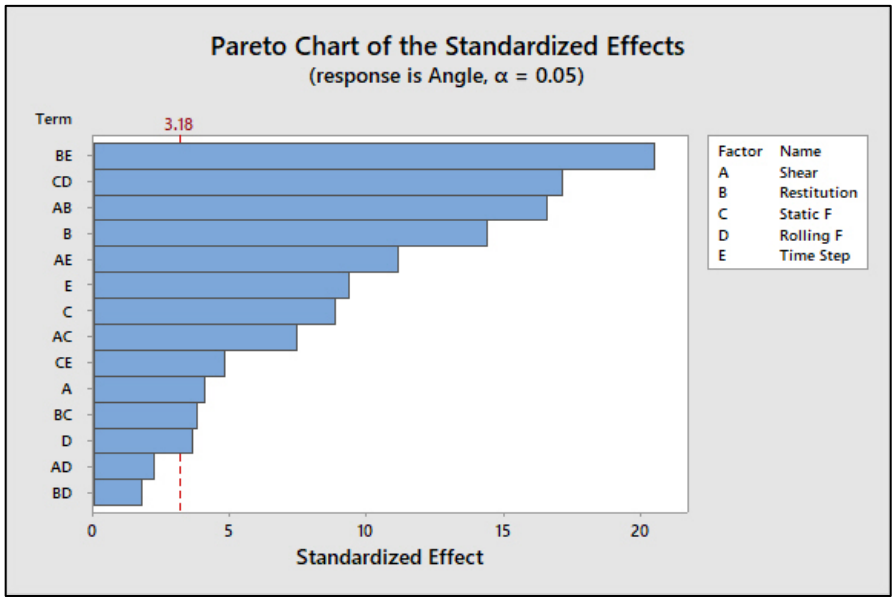

Figure 19: Particle to Particle Pareto Chart of Standardized Effects

From these results, Minitab calculated the regression equation that predicts the angle of repose from the level of each factor.

$$\text{Angle of Repose} = 27.332 - 2.507 \times X_1 - 8.920 \times X_2 + 3.163 \times X_3 + 1.287 \times X_4 + 5.795 \times X_5 + 10.270 \times X_1 * X_2 + 2.662 \times X_1 * X_3 + 0.788 \times X_1 * X_4 - 6.895 \times X_1 * X_5 + 1.350 \times X_2 * X_3 - 0.625 \times X_2 * X_4 - 12.707 \times X_2 * X_5 - 10.632 \times X_3 * X_4 - 1.725 \times X_3 * X_5$$

This regression equation has a R^2 value of 99.82%. This means that 99.82% of variation in the response is described by the model. This model fits our data extremely well.

The residual plots for the angle of repose are shown in Figure 20. The residual is the difference between the observed value, and the predicted value based on the regression equation [41]. To keep the calibration technique concise and realistic in length, all of the runs in this experiment were not replicated. This leaves most of the residuals to be 0, because of how well

the regression equation predicts the single run value [42]. However, the center point run was run four times, showing the variability that exists in the simulation. On all of the plots, the only residual points that are not 0 are from the center point runs. If all points were replicated, more variability in the system would be shown.

The Normal Probability Plot and Histogram show how much the data is normally distributed [41]. In the Normal Probability Plot the center point runs are scattered around the red line of best fit, showing that there is random variability in the system. The runs are not clumped together, showing no obvious underlying pattern. If the residuals fit a normal distribution, the histogram would look like a bell curve. The replicated center point runs are evenly random on both sides, suggesting that more data from more replicated runs would lead to a bell curve [41]. The Versus Fits and the Versus Order Plots prove if the residuals are scattered randomly around zero. Again, the center point runs show that the residuals are scattered randomly, displaying no outliers or other patterns in the data.

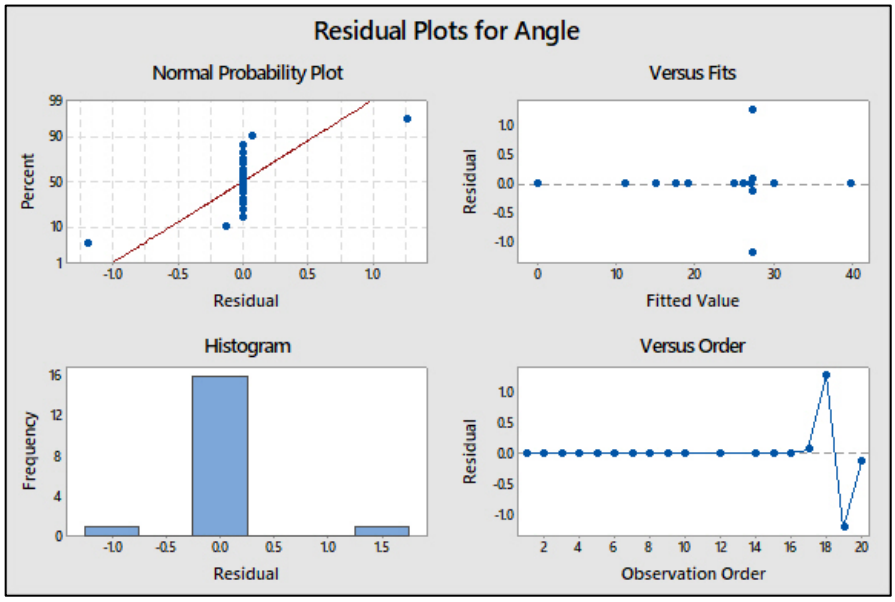

Figure 20: Particle to Particle Residual Plots for Effects

The results of the simulation runs were compared to the physical angle of repose test result to test the accuracy of the model. The physical angle of repose test resulted in an angle of repose of 31°. Run #15 was the closest run to achieving these results. The levels of this run are described in Table 16.

Table 16: Particle to Particle Most Accurate Simulation Run

	Shear Modulus (pascals)	Coefficient of Restitution	Coefficient of Static Friction	Coefficient of Rolling Friction	Time Step
Level	+	-	+	+	+
Value	2.65×10^{10}	0.1	0.9	0.195	80%

Since this run led to the most accurate angle of repose, the coefficient of restitution, the coefficient of static friction, and the coefficient of rolling friction for the particle to particle interactions were set to these levels for the entire particle to equipment DOE. A further look into the simulation time is done after calibrating the particle to equipment interactions.

5.2.2 Particle to Equipment Interaction Runs

The results of the particle to equipment interaction runs are in Table 17. Each angle was measured five times and averaged to get an accurate measurement. The estimated time it took the simulation to run is also outlined in the table. Again, the '---' represents a failed run. In this experiment all runs that had a low shear modulus and a high time step failed to run. As described in Section 5.2.1, this explains some of the limitations of the software.

Table 17: Particle to Equipment Interaction Run Results

Run #	Angle of Repose	Simulation Time (minutes)
1	7.0°	6
2	36.0°	250
3	30.2°	290
4	18.0°	6
5	39.0°	260
6	4.0°	6
7	13.0°	6
8	32.5°	300
9	33.6°	115
10	---	---
11	---	---
12	31.2°	80
13	---	---
14	30.8°	50
15	29.9°	73
16	---	---
17	23.2°	18
18	22.5°	19
19	22.3°	21
20	23.0°	17

The analysis of variance test with 95% confidence was completed for this data as well. The null and alternative hypothesis are below.

H_0: X_i or X_i X_j does not affect the angle of repose

H_1: X_i or X_i X_j affects the angle of repose

The results in Table 18 show that two of the main factors and most of the two-factor interactions are significant because their p-values are below 0.05.

Table 18: Particle to Equipment Main Effects Results

Factor	P-Value	Significant?
X_1	0.000	Yes
X_2	0.702	No
X_3	0.007	Yes
X_4	0.108	No
X_5	0.345	No

Table 19: Particle to Equipment Two-Factor Interaction Results

Interaction	P-Value	Significant?
$X_1 * X_2$	0.108	No
$X_1 * X_3$	0.000	Yes
$X_1 * X_4$	0.046	Yes
$X_1 * X_5$	0.006	Yes
$X_2 * X_3$	0.004	Yes
$X_2 * X_4$	0.005	Yes
$X_2 * X_5$	0.549	No

The Pareto Chart in Figure 21 visually shows the effects of each factor and interaction. This backs up the information found in Tables 18 and 19.

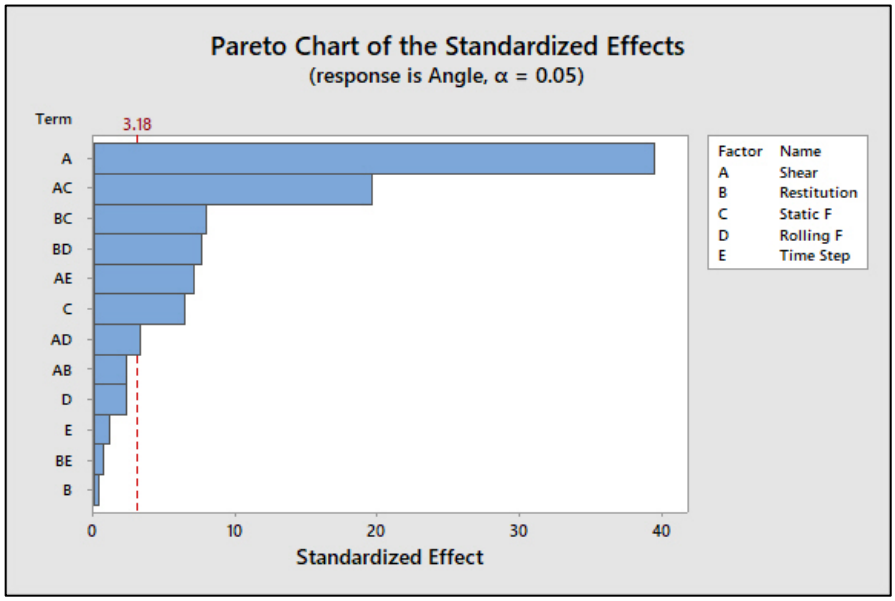

Figure 21: Particle to Equipment Pareto Chart of Standardized Effects

From these results, Minitab calculated the regression equation. This regression equation has an R^2 value of 99.97%, which fits the data extremely well. This means that 99.97% of variation in the response is described by the model.

$$\text{Angle of Repose} = 22.75 + 10.15 \times X_1 + 0.062 \times X_2 + 0.962 \times X_3 - 0.337 \times X_4 + 0.288 \times X_5 - 0.388 \times X_1 * X_2 - 2.912 \times X_1 * X_3 + 0.487 \times X_1 * X_4 - 1.813 \times X_1 * X_5 + 1.175 \times X_2 * X_3 - 1.125 \times X_2 * X_4 - 0.1 \times X_2 * X_5$$

The residual plots for the angle of repose are shown in Figure 22. Again, the residual is the difference between the observed value, and the predicted value based on the regression equation [41]. These plots also show that the replicated center point runs are evenly random for each plot. It is predicted if duplicate runs are performed on all effects, they would show more randomly distributed points that fit a normal distribution [41]. Again, the center point runs prove that the residuals are scattered randomly, showing no outliers or other patterns in the data.

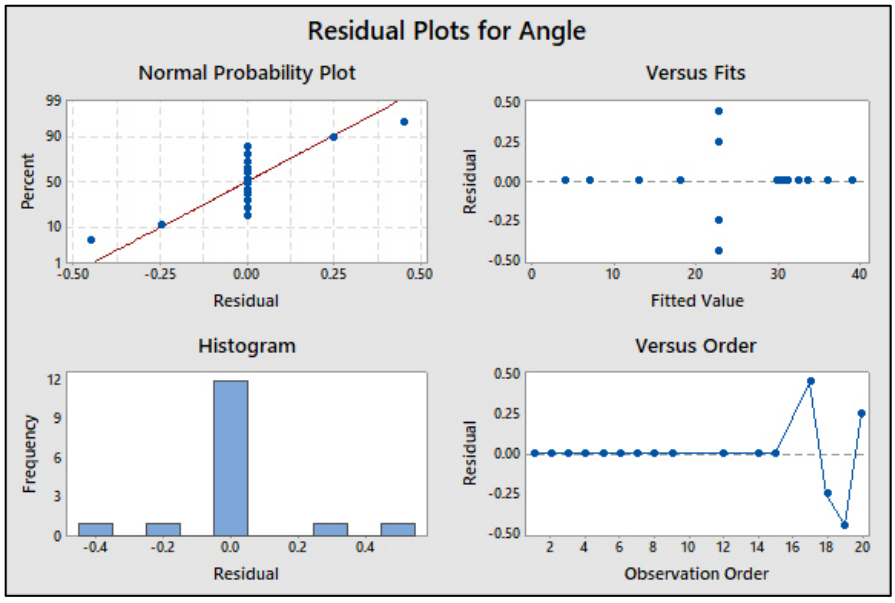

Figure 22: Particle to Equipment Residual Plots for Angle

The physical angle of repose test resulted in an angle of repose of 31°. Runs #12 and #14 were the closest runs to achieving these results and were off by only 0.2°. To determine which was the most accurate run, each angle was measured 15 more times, and then averaged. The angle for run 12 was averaged at 31.08°, and run 14 at 30.75°. These runs are both very accurate but run 12 was chosen as the best calibration for this powder because it was closest to 31°, the physical tested angle of repose. The levels of this runs are described in Table 20.

Table 20: Particle to Equipment Most Accurate Simulation Runs

	Shear Modulus (pascals)	**Coefficient of Restitution**	**Coefficient of Static Friction**	**Coefficient of Rolling Friction**	**Time Step**
Run 12					
Level	+	+	+	-	+
Value	2.65×10^{10}	0.9	0.9	0.05	80%

The time it takes a simulation to run depends on the computational power of the computer being used. If the computer is currently processing several other programs, the simulation time would be greater than if the computer was only running this software [26].

Looking at the results, the only inputs that significantly affected the simulation time were the shear modulus and the time step. This was predicted because the input coefficients only affect how the particles interact, not the process of how the DEM is calculated. Table 21 shows the most accurate angle of repose measured and the average simulation time for all possible combinations of these two inputs. This is based solely on the particle to equipment experiment.

Table 21: Angle of Repose and Simulation Time based on Shear Modulus and Time Step

Shear Modulus Level	Time Step Level	Angle of Repose (°)	Simulation Time (minutes)
+	+	31.08	79.5
+	-	30.2	275
-	+	18	6
-	-	23	18.75

As mentioned, decreasing the simulation time is a goal in calibration. These results show that the most accurate calibration has the actual shear modulus of the powder, and a time step that is closer to its nominal values T_R. In the future, these inputs could be kept constant, leaving a 2^3 factorial design of experiments. This DOE would require 8 less simulation runs, decreasing the calibration time more. A further investigation on this needs to be done.

5.3 Calibration Technique Summarized

The results show that this calibration technique can be used to calibrate a DEM simulation of the angle of repose test for metal PBF particles. The following summarizes the calibration process and should be used to calibrate additional materials in EDEM using a 50.0 scaled model. These results can then be used in future, larger calibrations.

1. Create a 50.0 scaled 3D model of the physical apparatuses used for the angle of repose test.
2. Import the model into EDEM and adjust all of the necessary EDEM inputs for the new powder. Refer to Section 4.4 for a thorough look on what inputs need to be changed. Ensure these inputs are scaled by 50.0 based on the scaling rules in Section 3.2.3.

3. Use the 2^{5-1} design of experiments with four center points to set up the experiment for both interactions. The DOE is shown in Table 22.

Table 22: DOE for Simulation

Run #	Shear Modulus	Coefficient of Restitution	Coefficient of Static Friction	Coefficient of Rolling Friction	Time Step
1	-	-	-	-	-
2	+	+	-	-	-
3	+	-	+	-	-
4	-	+	+	-	-
5	+	-	-	+	-
6	-	+	-	+	-
7	-	-	+	+	-
8	+	+	+	+	-
9	+	-	-	-	+
10	-	+	-	-	+
11	-	-	+	-	+
12	+	+	+	-	+
13	-	-	-	+	+
14	+	+	-	+	+
15	+	-	+	+	+
16	-	+	+	+	+
17	0	0	0	0	0
18	0	0	0	0	0
19	0	0	0	0	0
20	0	0	0	0	0

4. Run the particle to particle interaction experiment with the particle to equipment coefficients at their largest values. Run the experiment according to the following levels for each factor.

	Low Level (-)	Center Point (0)	High Level (+)
Shear Modulus	2.65×10^6	2.65×10^8	2.65×10^{10}
Coefficient of Restitution	0.1	0.5	0.9
Coefficient of Static Friction	0.1	0.5	0.9
Coefficient of Rolling Friction	0.05	0.1225	0.195
Time Step	20%	50%	80%

5. Measure the angle from each run five times, and average these to get the resultant angle.

6. Using the results, run an analysis of variance test in Minitab to see which factors and interactions are significant.
7. Compare all of the resultant angles to the measured angle of repose from the physical experiment for that powder to find the most accurate inputs. If two angles are equally similar, measure their angle 15 more times, and average them. Then compare these two angles to the physical angle again. Do this until one of the angles is more similar than the other.
8. Run the particle to equipment interaction experiment with the particle to particle inputs set as the inputs that yielded the most accurate angle from the last experiment.
9. Repeat steps 3 to 5. This results in the best inputs for both interactions for the simulation, providing a calibrated model.
10. Compare the accuracy of the angle of repose to the simulation time, based on the level of the shear modulus and time step. Make a judgment call as to whether to risk accuracy of the model for a decrease in simulation time.

Chapter 6

Recommendations and Future Work

After the experiment was concluded, more research on scaling DEM was conducted. It was found that scaling gravity in EDEM is advised [30]. This was overlooked in the beginning of this research. However, after the calibration was completed, more simulations were run to test if scaling of gravity really affects the output. The best simulation, run 12, was also run with the gravity scaled. Gravity is scaled by a factor of $\frac{1}{h}$ [30]. This is an inverse scale, so the higher the simulation is scaled, the lower the gravitational value will be. The two runs, one with the gravity scaled and one without the gravity scaled, resulted in angle of reposes that only differed by 1°. Additionally, the run with the gravity scaled took about 20 hours, compared to the four hours it took to run the simulation without gravity scaled. Further research on this is required to truly understand the effect of gravity on simulations.

This calibration technique outputs which level each input variable should be set at to most accurately simulate the angle of repose. For the shear modulus, the ideal value was 2.65×10^{10}, its high level for the experiment. However, the research shows that this shear modulus would be able to drop without affecting the resultant angle, to decrease the simulation time [29]. A robust parameter design is an experimental design used to find what settings the controllable factors should be set to in order to reduce the uncontrollable noise in the experiment [15]. This experimental design should be performed to attempt to decrease the shear modulus while keeping all other variables constant.

The calibration technique presented in this study can be used to calibrate any other powder in EDEM. Once powders are calibrated, further simulations can be done with these now understood particles. One goal is to eventually simulate the powder bed fusion process fully. The inputs generated for these powders in this calibration will be used as inputs for the full PBF simulation.

Appendix A

Scaling Factors for DEM [30]

Quantity name	Symbol	Dimensions	Scale factor (λ)	Category
Length	L	$[L]$	h	Basic
Time	T	$[T]$	h	Basic
Density	ρ	$[\rho]$	1	Basic
(Spatial) Position	X	$[L]$	h	Geometrical
Angular position, angle of rotation	θ	[1]	1	Geometrical
Area	A	$[L]^2$	h^2	Geometrical
Volume	V	$[L]^2$	h^3	Geometrical
Displacement, Overlap etc	u	$[L]$	h	Kinematic
Velocity	v	$[L][T]^{-1}$	1	Kinematic
Acceleration	a	$[L][T]^{-2}$	h^{-1}	Kinematic
Angular velocity	$\dot{\theta}$	$[T]^{-1}$	h^{-1}	Kinematic
Angular acceleration	$\ddot{\theta}$	$[T]^{-2}$	h^{-2}	Kinematic
(Natural) Frequency	ω	$[T]^{-1}$	h^{-1}	Dynamic
Force	F	$[\rho][L]^4[T]^{-2}$	h^2	Mechanical
Moment	Mo	$[\rho][L]^5[T]^{-2}$	h^3	Mechanical
Stiffness	k	$[\rho][L]^3[T]^{-2}$	h	Mechanical
Strain	ϵ	[1]	1	Mechanical
Stress	σ	$[\rho][L]^2[T]^{-2}$	1	Mechanical
Kinetic energy (volume) density	e_k	$[\rho][L]^2[T]^{-2}$	1	Mechanical
Strain energy (volume) density	e_s	$[\rho][L]^2[T]^{-2}$	1	Mechanical
Energy (volume) density	e	$[\rho][L]^2[T]^{-2}$	1	Mechanical
Mass	M	$[\rho][L]^3$	h^3	Material
Young's modulus	E	$[\rho][L]^2[T]^{-2}$	1	Material
Surface tension	κ	$[\rho][L]^3[T]^{-2}$	h	Material
Surface energy density	γ	$[\rho][L]^3[T]^{-2}$	h	Material
Viscosity (dynamic)	η	$[\rho][L]^2[T]^{-1}$	h	Material
Viscosity (kinematic)	ν	$[L]^2[T]^{-1}$	h	Material

Appendix B

T Value Table [39]

cum. prob	$t_{.50}$	$t_{.75}$	$t_{.80}$	$t_{.85}$	$t_{.90}$	$t_{.95}$	$t_{.975}$	$t_{.99}$	$t_{.995}$	$t_{.999}$	$t_{.9995}$
one-tail	0.50	0.25	0.20	0.15	0.10	0.05	0.025	0.01	0.005	0.001	0.0005
two-tails	1.00	0.50	0.40	0.30	0.20	0.10	0.05	0.02	0.01	0.002	0.001
df											
1	0.000	1.000	1.376	1.963	3.078	6.314	12.71	31.82	63.66	318.31	636.62
2	0.000	0.816	1.061	1.386	1.886	2.920	4.303	6.965	9.925	22.327	31.599
3	0.000	0.765	0.978	1.250	1.638	2.353	3.182	4.541	5.841	10.215	12.924
4	0.000	0.741	0.941	1.190	1.533	2.132	2.776	3.747	4.604	7.173	8.610
5	0.000	0.727	0.920	1.156	1.476	2.015	2.571	3.365	4.032	5.893	6.869
6	0.000	0.718	0.906	1.134	1.440	1.943	2.447	3.143	3.707	5.208	5.959
7	0.000	0.711	0.896	1.119	1.415	1.895	2.365	2.998	3.499	4.785	5.408
8	0.000	0.706	0.889	1.108	1.397	1.860	2.306	2.896	3.355	4.501	5.041
9	0.000	0.703	0.883	1.100	1.383	1.833	2.262	2.821	3.250	4.297	4.781
10	0.000	0.700	0.879	1.093	1.372	1.812	2.228	2.764	3.169	4.144	4.587
11	0.000	0.697	0.876	1.088	1.363	1.796	2.201	2.718	3.106	4.025	4.437
12	0.000	0.695	0.873	1.083	1.356	1.782	2.179	2.681	3.055	3.930	4.318
13	0.000	0.694	0.870	1.079	1.350	1.771	2.160	2.650	3.012	3.852	4.221
14	0.000	0.692	0.868	1.076	1.345	1.761	2.145	2.624	2.977	3.787	4.140
15	0.000	0.691	0.866	1.074	1.341	1.753	2.131	2.602	2.947	3.733	4.073
16	0.000	0.690	0.865	1.071	1.337	1.746	2.120	2.583	2.921	3.686	4.015
17	0.000	0.689	0.863	1.069	1.333	1.740	2.110	2.567	2.898	3.646	3.965
18	0.000	0.688	0.862	1.067	1.330	1.734	2.101	2.552	2.878	3.610	3.922
19	0.000	0.688	0.861	1.066	1.328	1.729	2.093	2.539	2.861	3.579	3.883
20	0.000	0.687	0.860	1.064	1.325	1.725	2.086	2.528	2.845	3.552	3.850
21	0.000	0.686	0.859	1.063	1.323	1.721	2.080	2.518	2.831	3.527	3.819
22	0.000	0.686	0.858	1.061	1.321	1.717	2.074	2.508	2.819	3.505	3.792
23	0.000	0.685	0.858	1.060	1.319	1.714	2.069	2.500	2.807	3.485	3.768
24	0.000	0.685	0.857	1.059	1.318	1.711	2.064	2.492	2.797	3.467	3.745
25	0.000	0.684	0.856	1.058	1.316	1.708	2.060	2.485	2.787	3.450	3.725
26	0.000	0.684	0.856	1.058	1.315	1.706	2.056	2.479	2.779	3.435	3.707
27	0.000	0.684	0.855	1.057	1.314	1.703	2.052	2.473	2.771	3.421	3.690
28	0.000	0.683	0.855	1.056	1.313	1.701	2.048	2.467	2.763	3.408	3.674
29	0.000	0.683	0.854	1.055	1.311	1.699	2.045	2.462	2.756	3.396	3.659
30	0.000	0.683	0.854	1.055	1.310	1.697	2.042	2.457	2.750	3.385	3.646
40	0.000	0.681	0.851	1.050	1.303	1.684	2.021	2.423	2.704	3.307	3.551
60	0.000	0.679	0.848	1.045	1.296	1.671	2.000	2.390	2.660	3.232	3.460
80	0.000	0.678	0.846	1.043	1.292	1.664	1.990	2.374	2.639	3.195	3.416
100	0.000	0.677	0.845	1.042	1.290	1.660	1.984	2.364	2.626	3.174	3.390
1000	0.000	0.675	0.842	1.037	1.282	1.646	1.962	2.330	2.581	3.098	3.300
z	0.000	0.674	0.842	1.036	1.282	1.645	1.960	2.326	2.576	3.090	3.291
	0%	50%	60%	70%	80%	90%	95%	98%	99%	99.8%	99.9%
	Confidence Level										

BIBLIOGRAPHY

[1] King, W. E., Anderson, A.T., Ferencz, R.M.m Hodge, N.E., Kamath, C., Khairallah, S.A., and Rubenchik, A.M. *Laser Powder Bed Fusion Additive Manufacturing of Metals; Physics, Computational, and Materials Challenges.* Applied Physics Reviews, vol. 2, no. 4, 2015, p. 041304., doi:10.1063/1.4937809.

[2] "Additive Manufacturing vs Subtractive Manufacturing." *Creative Mechanisms*, 2016.

[3] "7 Families of Additive Manufacturing." *Hybrid Manufacturing Technologies*, www.hybridmanutech.com/resources.html.

[4] "Powder Bed Fusion." *Additive Manufacturing Research Group*, Loughborough University.

[5] Snow, Zachary. The Pennsylvania State University Department of Industrial and Manufacturing Engineering, 12 March 2018, The Pennsylvania State University.

[6] Zhao, Cang, Fezzaa, Kamel, Cunningham, Ross, Wen, Haidan, De Carlo, Francesco, Chen, Lianyi, Rollett, Anthony, and Sun, Tao. "Real-Time Monitoring of Laser Powder Bed Fusion Process Using High-Speed X-Ray Imaging and Diffraction." Docphin, Scientific Reports, 15 June 2017, www.docphin.com.

[7] Frazier, William E. "Metal Additive Manufacturing: A Review." *Journal of Materials Engineering and Performance*, vol. 23, no. 6, June 2017, doi:10.1007.

[8] A. Sutton, C. Kriewall, M. Leu, J. Newkirk, *Powders for Additive Manufacturing Processes: Characterization Techniques and Effect on Part Properties.* Department of Materials Science and Engineering, Missouri University of Science and Technology, 2016.

[9] Slotwinski, J. A., Garboczi, E. J., Stutzman, P. E., Ferraris, C. F., Watson, S. S., and Peltz, M. A. "Characterization of Metal Powders Used for Additive Manufacturing." *Journal of Research of the National Institute of Standards and Technology*, vol. 119, 2014, pp. 460–493., doi:10.6028.

[10] "Standard Guide for Characterizing Properties of Metal Powders Used for Additive Manufacturing Processes." *Research of the National Institute of Standards and Technology*, vol. 119, 2014, doi:10.1520/f3049.

[11] Palumbo, Biagio, Del Re, Francesco, Martorelli, Massimo, Lanzotti, Antonia, and Corrado, Pasquale. "Tensile Properties Characterization of AlSi10Mg Parts Produced by Direct Metal Laser Sintering via Nested Effects Modeling." University of Naples Federico, MDPI, 2017.

[12] Parteli, Eric J.r., and Thorsten Poschel. "Particle-Based Simulation of Powder Application in Additive Manufacturing." *Powder Technology*, vol. 288, 2016, pp. 96–102., doi:10.1016/j.powtec.2015.10.035.

[13] Balevicius, R, Kacianauskas, R, Mroz, Z, and Sielamowicz, I. “Microscopic and Macroscopic Analysis of Granular Material Behaviour in 3D Flat-Bottomed Hopper by the Discrete Element Method.” *Archives of Mechanics*, 25 Apr. 2007, yadda.icm.edu.pl.

[14] Bolintineanu, Dan, and Lechman, Jeremy B. *Simulations of powder bed formation for additive manufacturing*. United States: N. p., 2015. Web.

[15] Sousani, Marina. What Is DEM – an Introduction to the Discrete Element Method. *EDEM Simulations*, Jan. 2018.

[16] Montgomery, Douglas. “The 2^k Factorial Design.” *Design and Analysis of Experiments*, Eighth ed., John Wiley & Sons, 2013, pp. 233–303.

[17] “A Glossary of DOE Terminology.” *National Institute of Standards and Technology*, Engineering Statistics Handbook, www.itl.nist.gov.

[18] “Errors and Error Estimation.” *First Year Physics Laboratory Manual*, School of Physics - Sydney, Australia, unsw.edu.au.

[19] “Central Composite Designs (CCD)” *National Institute of Standards and Technology*, Engineering Statistics Handbook, www.itl.nist.gov.

[20] Frankowski, Piotr, and Martin Morgeneyer. “Calibration and Validation of DEM Rolling and Sliding Friction Coefficients in Angle of Repose and Shear Measurements.” *EDEM Simulation*, American Institute of Physics, 2013, www.edemsimulation.com.

[21] Quist, Johannes, and Magnus Evertsson. “Framework for DEM Model Calibration and Validation.” Core.ac.uk, Department of Product and Production Development, Chalmers University of Technology, 7 Oct. 2017, publications.lib.chalmers.se

[22] Grima, Andrew Phillip, and Peter Wilhelm Wypych. “Development and Validation of Calibration Methods for Discrete Element Modelling.” *Granular Matter*, vol. 13, no. 2, 23 July 2010, pp. 127–132., doi:10.1007/s10035-010-0197-4.

[23] Li, Qiang, Feng, Mingxia, Zou, Zongshu. “Validation and Calibration Approach for Discrete Element Simulation of Burden Charging in Pre-Reduction Shaft Furnace of COREX Process.” *ISIJ International*, vol. 53, no. 8, 22 May 2013, pp. 1265–1371.

[24] Mei, Lei, Hu, Jiquan, Yang, Jianguo, and Yuan Jianming. “Research on Parameters of EDEM Simulations Based on the Angle of Repose Experiment.” 2016 IEEE 20th International Conference on Computer Supported Cooperative Work in Design (CSCWD), 2016, doi:10.1109/cscwd.2016.7566053.

[25] Gkeka, Paraskevi. “Molecular Dynamics Studies of Peptide-Membrane Interactions: Insights from Coarse-Grained Models.” University of Edinburgh, 2010, pp. 49–51.

[26] EDEM 2.4 User Guide. EDEM 2.4 User Guide, *DEM Solutions*, 2011.

[27] Roux, Sébastien Le. “Model Box Periodic Boundary Conditions - P.B.C.” *Periodic Boundary Conditions*, isaacs.sourceforge.net/phys/pbc.html.

[28] Moebs, William, and Jeff Sanny. “Static Equilibrium and Elasticity.” *University Physics*, edited by Samuel J Ling, vol. 1, OpenStax, pp. 609–619.

[29] Cole, Stephen. “Particle Shear Modulus - It Can Save You Time.” *EDEM Simulation*, 28 July 2015, edemsimulation.com.

[30] Feng, Y. T., and D. R. J. Owen. “Discrete Element Modelling of Large Scale Particle Systems-I: Exact Scaling Laws.” *Computational Particle Mechanics*, vol. 1, no. 2, 2014, pp. 159–168., doi:10.1007/s40571-014-0010-y.

[31] ASTM C1444-00, “Standard Test Method for Measuring the Angle of Repose of Free-Flowing Mold Powders” (Withdrawn 2005), *ASTM International*, West Conshohocken, PA, 2000, www.astm.org

[32] ASTM B213-17, “Standard Test Methods for Flow Rate of Metal Powders Using the Hall Flowmeter Funnel”, *ASTM International*, West Conshohocken, PA, 2017, www.astm.org

[33] Zeng, Xian Ming, Martin, Gary, and Marriott, Christopher. “Particulate Interactions in Dry Powder Formulation for Inhalation.” *Semantic Scholar*, 2001, pdfs.semanticscholar.org.

[34] “Angle of Repose Simulation - with Inter Particle Cohesion.” YouTube, *EDEM Simulation*, 2 July 2013, www.youtube.com/watch?v.

[35] Vail, Jane. “The Angle of Repose.” *Wallis Engineering RSS*, walliseng.net.

[36] Peng, Bo. “Discrete Element Method (DEM) Contact Models Applied to Pavement Simulation.” Virginia Polytechnic Institute and State University, 2013, pp. 19–26.

[37] Kelly. “The Linear Elastic Model.” *Solid Mechanics Part I*, 2015, pp. 145–153.

[38] Khan, Hiba, and Jonathan Tod Pittam. “Force Displacement Model.” *DEM Analysis of Lateral Earth Pressure*, University of Edinburgh, demlateralearthpressure.weebly.com.

[39] “T Value Table.” T Table, www.ttable.org/.

[40] “Effects Plots for Analyze Factorial Design.” Minitab, support.minitab.com

[41] “Residual Plots in Minitab.” Minitab, support.minitab.com

[42] Chandra, Jaya. The Pennsylvania State University Department of Industrial and Manufacturing Engineering, 20 March 2018, The Pennsylvania State University.

ACADEMIC VITA

Kristen N. Meihofer

10 Pheasant Drive, Holland, PA 18966
267-438-4227 – kristenmeihofer@gmail.com
www.linkedin.com/in/kristen-meihofer

Education

The Pennsylvania State University – Schreyer Honors College *Spring 2018*
B.S. in Industrial Engineering
Engineering Leadership Development Minor

Work Experience

Danaher Corporation, Beckman Coulter Diagnostics – Chaska, MN *May 2016 – August 2016*
Manufacturing Engineering Intern (40 hours/week)

- Applied Lean Manufacturing tools to reduce the filling line changeover time by 70%
- Developed process improvements to reduce the reject rate by 50% and eliminate muda (waste)
- Evaluated the line productivity and customer demand to optimize the Kanban system for inventory control

Danaher Corporation, Pall Life Sciences – Westborough, MA *May 2017 – August 2017*
Process Engineer / Project Manager Intern (40 hours/week)

- Managed the suppliers and designers of an automated filtration system project for a biopharmaceutical compan
- Led weekly 3D model review meetings with the customer and revised the CAD model per updates
- Negotiated material quotes with vendors to optimize revenue and achieve 35% overall profit

Research Experience

Penn State Undergraduate Research Program – University Park, PA
Powder Characterization Techniques Researcher (10 hours/week) *August 2017 – Present*

- Studying the application of the Discrete Element Method (DEM) for granular material in 3D printing
- Calibrating a DEM model for a powder characterization test
- Composing an independent honors thesis to be published in April, 2017

Sports Analytics Researcher (10 hours/week) *August 2016 – May 2017*

- Analyzed volleyball data in Matlab to summarize and develop relationships among hits, plays, and positions
- Employed a logistical regression model to graph various probabilities of success to help develop team strategies

Leadership Experience

Penn State Engineering Ambassador Network *April 2015 – Present*
Engineering Ambassador (5 hours/week)

- Representing the College of Engineering through professional development events and technical presentations
- Presenting to prospective students and leading tours and outreach events to inspire youth into the STEM fields

Penn State IFC/Panhellenic Dance Marathon (THON) *September 2017 – Present*
OPPerations Captain (20 hours/week)

- Planning logistics for several events to raise funds and awareness for the fight against pediatric cancer
- Leading a 37 person committee of enthusiastic volunteers to ensure all events run smoothly and efficiently

Penn State Engineering Leadership Development Minor *May 2016 – May 2017*
Marketing/Administrative Intern (10 hours/week)

- Introduced and implemented marketing strategies for the minor and master programs to increase enrollment
- Developed and delivered presentations to over 900 students to engage undergraduates into the program

Skills

- Software: SolidWorks, Matlab, Minitab
- Lean Manufacturing Tools: Kaizen, Value Stream Mapping, Standard Work, Kanban, 5S

Honors

- William and Wyllis Leonhard Honors Program
- Marcus Industrial Engineering Endowment
- Phillip Seville Outstanding Community Service Award
- Penn State President Sparks and Freshman Award